Anticlockwise metamorphic pressure–temperature paths and nappe stacking in the Reisa Nappe Complex in the Scandinavian Caledonides, northern Norway: evidence for weakening of lower continental crust before and during continental collision

Carly Faber, Holger Stünitz, Deta Gasser, Petr Jeřábek, Katrin Kraus, Fernando Corfu, Erling K Ravna, Jiří Konopásek

Solid Earth, 10, 117–148, 2019
https://doi.org/10.5194/se-10-117-2019

Solid Earth Open Access EGU

Anticlockwise metamorphic pressure–temperature paths and nappe stacking in the Reisa Nappe Complex in the Scandinavian Caledonides, northern Norway: evidence for weakening of lower continental crust before and during continental collision

Carly Faber[1], Holger Stünitz[1,2], Deta Gasser[3,4], Petr Jeřábek[5], Katrin Kraus[1], Fernando Corfu[6], Erling K. Ravna[1], and Jiří Konopásek[1]

[1]Department of Geosciences, UiT The Arctic University of Norway, Tromsø 9037, Norway
[2]Institut des Sciences de la Terre (ISTO), Université d'Orleans, Orleans 45100, France
[3]Western Norway University of Applied Sciences, Sogndal 6851, Norway
[4]Geological Survey of Norway, Trondheim 7491, Norway
[5]IPSG, Faculty of Science, Charles University, Albertov 6, 128 43, Prague 2, Czech Republic
[6]Department of Geosciences and Centre for Earth Evolution and Dynamics, University of Oslo, Oslo, Norway

Correspondence: Carly Faber (carlyfaber1@gmail.com)

Received: 26 July 2018 – Discussion started: 31 July 2018
Revised: 16 December 2018 – Accepted: 17 December 2018 – Published: 17 January 2019

Abstract. This study investigates the tectonostratigraphy and metamorphic and tectonic evolution of the Caledonian Reisa Nappe Complex (RNC; from bottom to top: Vaddas, Kåfjord, and Nordmannvik nappes) in northern Troms, Norway. Structural data, phase equilibrium modelling, and U-Pb zircon and titanite geochronology are used to constrain the timing and pressure–temperature (P–T) conditions of deformation and metamorphism during nappe stacking that facilitated crustal thickening during continental collision. Five samples taken from different parts of the RNC reveal an anticlockwise P–T path attributed to the effects of early Silurian heating (D_1) followed by thrusting (D_2). At ca. 439 Ma during D_1 the Nordmannvik Nappe reached the highest metamorphic conditions at ca. 780 °C and ∼ 9–11 kbar inducing kyanite-grade partial melting. At the same time the Kåfjord Nappe was at higher, colder, levels of the crust ca. 600 °C, 6–7 kbar and the Vaddas Nappe was intruded by gabbro at > 650 °C and ca. 6–9 kbar. The subsequent D_2 shearing occurred at increasing pressure and decreasing temperatures ca. 700 °C and 9–11 kbar in the partially molten Nordmannvik Nappe, ca. 600 °C and 9–10 kbar in the Kåfjord Nappe, and ca. 640 °C and 12–13 kbar in the Vaddas Nappe. Multistage titanite growth in the Nordmannvik Nappe records this evolution through D_1 and D_2 between ca. 440 and 427 Ma, while titanite growth along the lower RNC boundary records D_2 shearing at 432±6 Ma. It emerges that early Silurian heating (ca. 440 Ma) probably resulted from large-scale magma underplating and initiated partial melting that weakened the lower crust, which facilitated dismembering of the crust into individual thrust slices (nappe units). This tectonic style contrasts with subduction of mechanically strong continental crust to great depths as seen in, for example, the Western Gneiss Region further south.

1 Introduction

Large-scale thrusting and nappe stacking are the main processes responsible for crustal shortening during continental collision. Crustal rocks can be subducted to depths of ∼ 200 km (e.g. Chopin, 2003; Spengler et al., 2009; Hacker et al., 2010), or be included in large-scale nappe stacks (e.g. Escher et al., 1993; Escher and Beaumont, 1997). The crucial factor that controls the style of large-scale deformation and whether rocks are subducted or are stacked in mid- to lower-crustal ductile nappe piles is the rheology, which is dependent on temperature, availability of fluids, composition

of the rocks involved, and the presence or absence of melt (e.g. Hollister and Crawford, 1986; Beaumont et al., 2006; Gerya and Meilick, 2010; Labrousse et al., 2010; Jeřábek et al., 2012). The immediate pre-collisional history of rocks involved in nappe stacking plays a significant role in determining these factors. In active continental collision zones such as the Himalaya, mid- and lower-crustal processes are generally inferred from surface deformation, geophysical information, and the geochemistry of erupted volcanic rocks (e.g. Schulte-Pelkum et al., 2005; Zhao et al., 2009). In contrast, older and deeply eroded continental collision zones such as the Caledonides allow for direct study of nappe thrusting at mid- and lower-crustal levels, allowing for insight into the high-temperature processes of large-scale continental subduction and crustal shortening. The nappe concept of large-scale thrust units was developed in the Alps (Bertrand, 1884; Schardt, 1893). The nappe units were defined on the basis of stratigraphy (in the sediments), or, in higher-grade metamorphic "basement" units, by nappe dividers of cover sediments between these (e.g. Pfiffner, 2016). When the metamorphic temperatures during thrusting are high in all units, the distinction between basement and cover units becomes virtually impossible. Under such high-grade conditions, the thrust units typically are thin parallel rock slices of variable extent, and the distinction of individual nappe units can only be made on the basis of metamorphic grade or age of metamorphism and deformation. This is the situation in the western part of the northern Caledonides, where only high-grade rocks of the deep part of the orogen form the nappe stack.

The Caledonides were formed by convergence and collision between Baltica and Laurentia in Silurian to Devonian times (Fig. 1a). The resulting large-scale nappe stacks provide access to the study of mid- to lower-crustal processes during a continental collision of Himalayan style and extent (e.g. Streule et al., 2010; Labrousse et al., 2010). In northern Norway, a well preserved section, from the autochthonous Baltica basement to exotic terranes and ophiolites, is exposed (Fig. 1b), displaying large gradients in metamorphic grade and deformational style (Corfu et al., 2014). The Reisa Nappe Complex (RNC) represents a large viscously deformed nappe stack, metamorphosed at amphibolite- to granulite-facies conditions, displaying pervasive deformation and possible Caledonian partial melting (Roberts and Sturt, 1980; Andresen, 1988). Based on its similarity to rocks at the same tectonostratigraphic level (e.g. the Magerøy Nappe, located in northern Finnmark; Andersen et al., 1982; Corfu et al., 2006), the RNC is considered equivalent to other Iapetus-derived or outer Baltica margin (upper allochthon) units in the Caledonides. It may also preserve an early Silurian history, recording events immediately prior to or during early continental collision between Baltica and Laurentia (e.g. Andréasson et al., 2003; Slagstad and Kirkland, 2018). In addition, its tectonostratigraphic position directly below the ophiolitic rocks of the Lyngsfjellet Nappe places it in a distinctive palaeogeographic position. Understanding the structure and composition of the RNC together with its metamorphic, deformation, and magmatic history will help to establish how lower-crustal nappe stacking during continental collision takes effect. The pre-Caledonian and Caledonian evolution of the rocks affected the deformation behaviour during nappe stacking in this particular part of the Caledonian orogen.

2 Geological framework

The Scandinavian Caledonides consist of a series of allochthonous nappes, with, from bottom to top, Baltican, Iapetus, and Laurentian affinities (Roberts and Gee, 1985; Stephens and Gee, 1989; Fig. 1a).

2.1 The north Norwegian Caledonides

In northern Norway, the Baltican basement with its metasedimentary autochthonous cover is overlain by the parautochthonous metasedimentary rocks of the Gaissa Nappe Complex (Fig. 1b; e.g. Ramsay et al., 1985). Above these, the allochthonous rocks form a nappe stack including the following units from bottom to top: (1) the metasedimentary and metaigneous rocks of the Kalak Nappe Complex (KNC), (2) the metasedimentary and metaigneous rocks of the RNC, (3) the ophiolitic and metasedimentary rocks of the Lyngsfjellet Nappe, (4) gneisses and migmatites of the Nakkedalen Nappe, and (5) metasedimentary rocks of the Tromsø Nappe (Fig. 1b; Andresen, 1988; Kvassnes et al., 2004; Kirkland et al., 2006, 2007a; Augland et al., 2014; Rice, 2014; Gee et al., 2017). Caledonian metamorphic conditions associated with nappe thrusting generally increase upwards through the KNC and RNC, from low greenschist facies in the parautochthonous metasediments to upper amphibolite or lower granulite facies at the top of the RNC, with local granulite facies metamorphism generally interpreted to be pre-Caledonian (Andresen, 1988; Elvevold et al., 1993, 1994;). The Lyngsfjellet Nappe displays greenschist facies metamorphism at its base with higher-grade metamorphism in the overlying metasediments, and the overlying Nakkedalen and Tromsø nappes show amphibolite to eclogite facies metamorphism (Andresen and Bergh, 1985; Andresen and Steltenpohl, 1994; Corfu et al., 2003). The predominant Caledonian deformation, associated with continental collision (often referred to as Scandian; e.g. Corfu et al., 2014) in the allochthons in northern Norway is associated with top-to-SE and top-to-E shearing (Rice, 1998).

The palaeogeographic origin of several of the Caledonian nappes in northern Norway is debated. The Gaissa Nappe Complex is interpreted to represent telescoped Baltica margin cover, and the KNC has traditionally also been interpreted to represent more outboard Baltica basement rocks and its late Precambrian to Paleozoic cover (e.g. Stephens and Gee, 1989; Gee et al., 2017). However, recent evidence

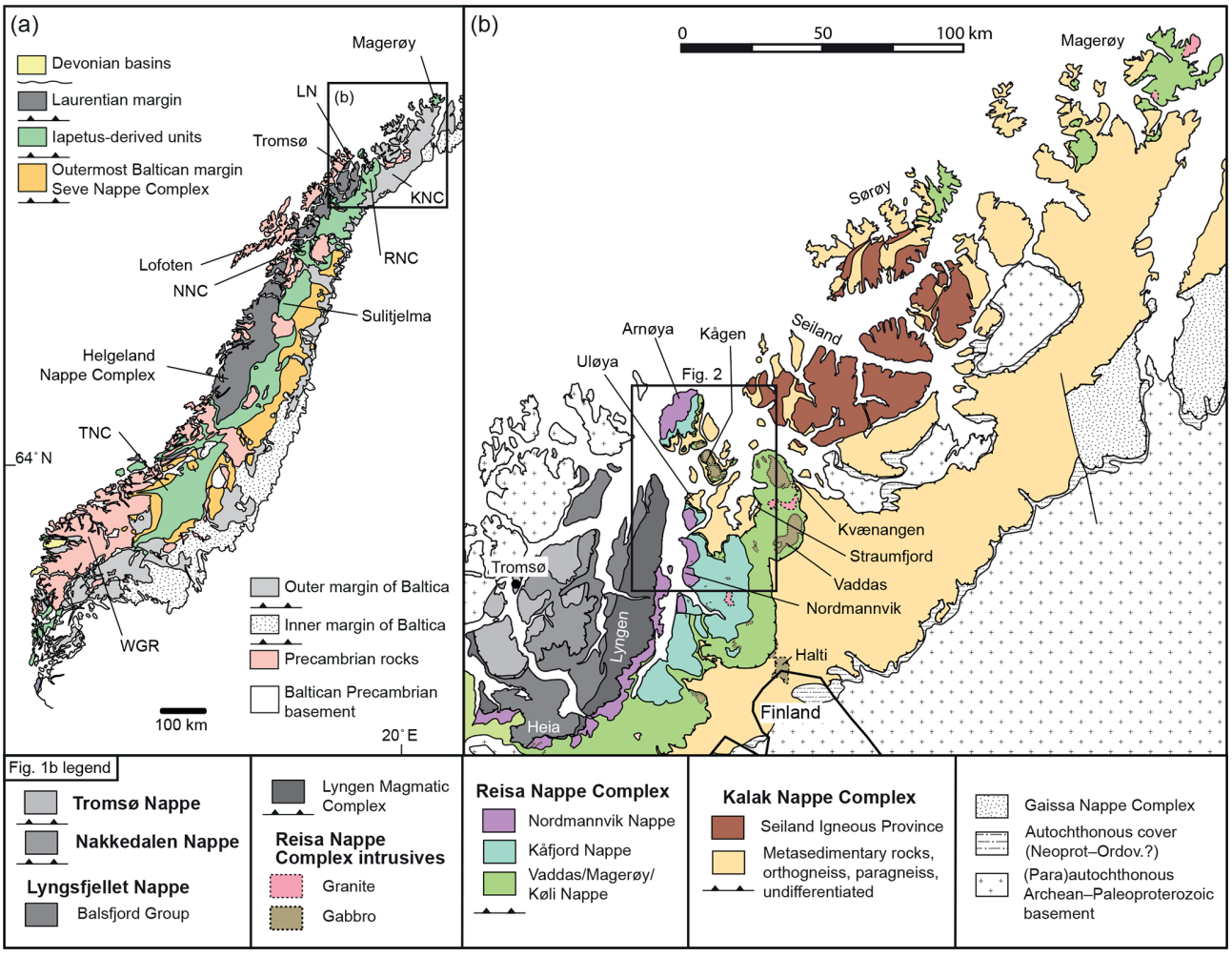

Figure 1. (a) Simplified map of the Scandinavian Caledonides and their inferred palaeotectonic origin, modified from Gee et al. (2010). LN is the Lyngsfjellet Nappe, WGR is the Western Gneiss Region, NNC is the Narvik Nappe Complex, KNC is the Kalak Nappe Complex, RNC is the Reisa Nappe Complex, and TNC is the Trondheim Nappe Complex. **(b)** Map showing the extent of the Reisa Nappe Complex in northern Norway, based on Zwaan (1988) and own correlations. The Vaddas, Kåfjord, and Nordmannvik nappes are shown in colour. The study area is denoted by the black box (Fig. 2).

shows that the sedimentary cover in the KNC had already been deposited between 1000 and 900 Ma, and the KNC underwent metamorphism, deformation, and magmatism during several events at about 970–950, 870–830, 700, 600, and 570 Ma (Daly et al., 1991; Kirkland et al., 2006; Corfu et al., 2007, 2011). These Neoproterozoic events are not known in the Baltica basement elsewhere, implying that either the KNC has an exotic origin or that a still unknown type of suture (typical suture rocks are lacking beneath the KNC) separated it from the Archean–Paleoproterozoic northern Baltic basement before the final collision (e.g. Kirkland et al., 2006, 2007a, b, 2008; Corfu et al., 2007, 2011). The RNC has previously been interpreted to represent either Iapetus-derived or outermost Baltican rocks, whereas the Lyngsfjellet Nappe is traditionally considered as Iapetus-derived, marking the transition towards the Laurentia-derived Nakkedalen and Tromsø nappes (e.g. Stephens and Gee, 1989; Corfu et al., 2003).

2.2 The Reisa Nappe Complex (RNC)

The RNC crops out east of Lyngen (Fig. 1b) and includes, from bottom to top, the Vaddas, Kåfjord, and Nordmannvik nappes (Figs. 1, 2; Zwaan and Roberts, 1978; Zwaan, 1988). The Vaddas Nappe has been divided into lower and upper parts (Fig. 3; Lindahl et al., 2005). The lower part (lower Vaddas) is mapped only between Straumfjord and Kvænangen and includes a basal marble and calc-silicate layer, garnet- and graphite-bearing schist, metaarkose, quartzite, and amphibolite representing metamorphosed volcano-sedimentary rocks and turbidites (Andresen, 1988; Lindahl et al., 2005). The 602 ± 5 Ma Rappesvarre

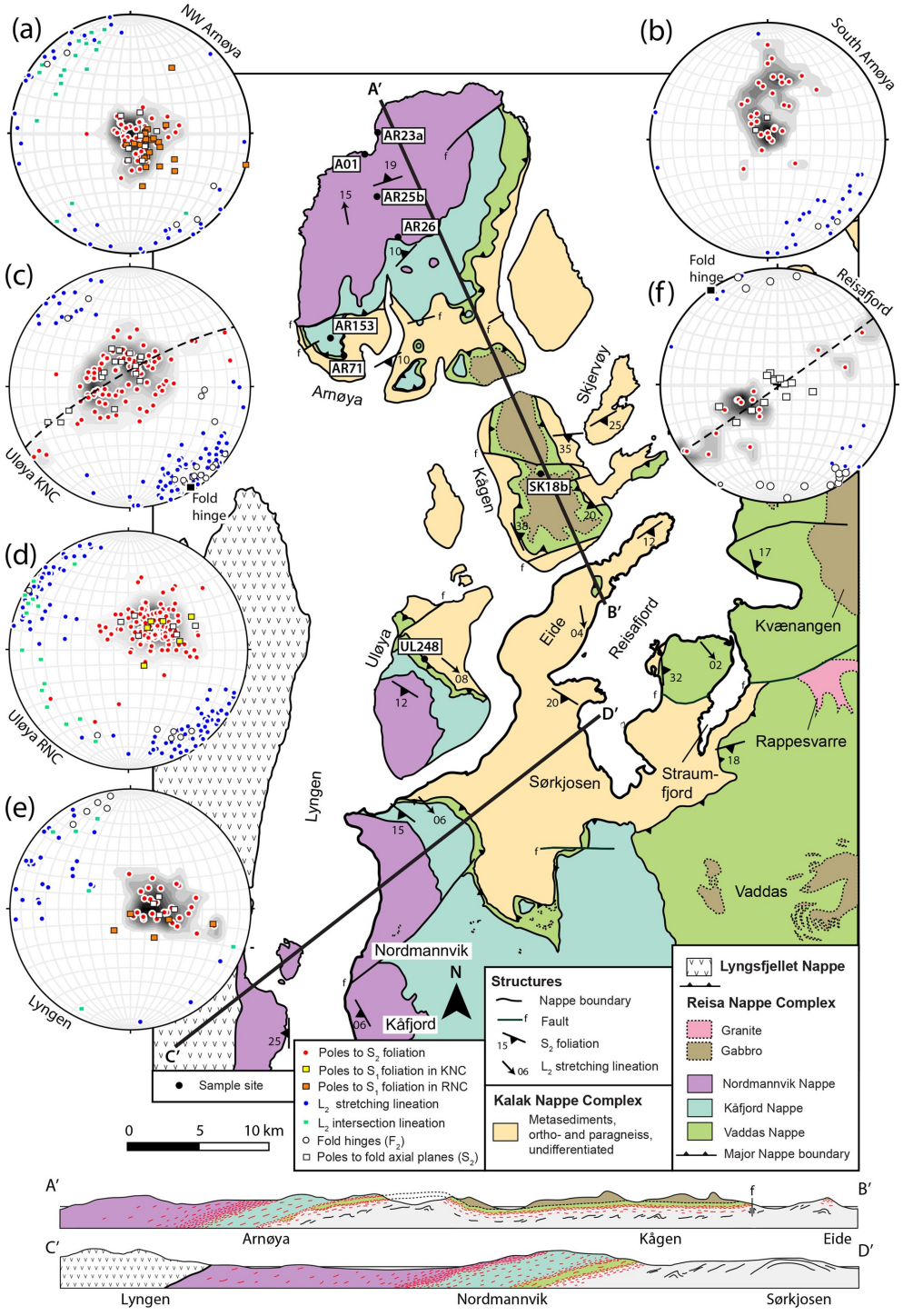

Figure 2. Structural map, stereonets, and cross sections from the study area. Petrological and geochronological sample locations are indicated. Structures are shown on equal area lower hemisphere stereographic projections as follows: **(a)** the RNC on northern and western Arnøya, **(b)** the RNC on southernmost Arnøya, **(c)** the KNC on Uløya; poles to S_2 plot on a great circle (dashed line), the pole of which (black box) defines a fold hinge parallel to plotted stretching lineations, **(d)** the RNC on Uløya, **(e)** the Nordmannvik Nappe on the eastern coast of Lyngen, and **(f)** the Vaddas Nappe on the eastern side of Reisafjord; poles to foliation define a folding event with the fold hinge (black box) parallel to the L_2 stretching lineation and measured axes of open folds. Cross sections are shown at the bottom of the figure from Arnøya to Eide **(A'–B')** and from Lyngen to Sørkjosen **(C'–D')**. The density of red lines corresponds to the intensity of ductile deformation within and along boundaries between individual nappes. Caledonian foliations are shown in red, whereas black ones are possibly older.

metagranite occurs in the lower Vaddas Nappe, although its relationship with the surrounding rocks is unclear. It appears to be equivalent to rocks in the Corrovarre Nappe, at the top of the KNC (Figs. 2, 3; Lindahl et al., 2005; Corfu et al., 2007; Gee et al., 2017).

The base of the upper part of the Vaddas Nappe (upper Vaddas) includes a quartzite conglomerate and marble layer with local Late Ordovician–early Silurian fossils (447–441 Ma; Fig. 3; Binns and Gayer, 1980). Above, garnet-bearing calc-schist with layers and lenses of amphibolite underlie a thick sequence of metapsammites (Zwaan, 1988; Lindahl et al., 2005). Several undated tholeiitic gabbro bodies intrude the upper Vaddas rocks (Kågen, Kvænangen and Vaddas gabbros, Figs. 2, 3; Lindahl et al., 2005). The Halti Igneous Complex (Fig. 1b), a klippe of the Vaddas Nappe (Vaasjoki and Sipilä, 2001), but also interpreted as an intrusion in the KNC (Andréasson et al., 2003), yields intrusion ages of 434 ± 5 and 438 ± 5 Ma. The Magerøy Nappe and Hellefjord schists in the north-east and Køli Nappe in the south-west are thought to be equivalents of the Vaddas Nappe (Fig. 1b; Gayer and Roberts, 1973; Andersen, 1981; Lindahl et al., 2005; Corfu et al., 2006, 2011; Kirkland et al., 2005, 2016). Volcaniclastic and intrusive rocks in the Magerøy Nappe give early Silurian ages (442–435 Ma) suggesting almost synchronous deposition and intrusion (Robins, 1998; Corfu et al., 2006, 2011; Kirkland et al., 2005, 2016).

Both the Vaddas and Kåfjord nappes display amphibolite facies metamorphic conditions and pervasive shearing. They are separated by a mylonite zone (Zwaan and Roberts, 1978; Andresen, 1988; Zwaan, 1988). The lower part of the Kåfjord Nappe is composed of marble and calc-schist, metapsammite and garnet mica-schist. Mylonitic gneisses with boudinaged amphibolite and granitic bodies dominate the upper part of the nappe (Andresen, 1988). Small gabbro bodies of unknown age also occur (Zwaan, 1988). A Rb-Sr whole-rock age from the upper part of the nappe suggests anatexis and granite crystallization at 440 Ma (Dangla et al., 1978). The boundary between the Kåfjord and the overlying Nordmannvik Nappe is a well developed mylonitic zone (Andresen, 1988). The Nordmannvik Nappe, defined east of Lyngen at Nordmannvik and best studied from Nordmannvik to Heia (Fig. 1b), is a polymetamorphic nappe showing a pervasive amphibolite facies foliation surrounding granulite facies relict lenses (Elvevold, 1987; Andresen, 1988; Zwaan, 1988; Lindstrøm and Andresen, 1992; Augland et al., 2014). The nappe is comprised of garnet-mica-schist and gneiss, migmatite, minor calc-silicate, amphibolite, and marble (Fig. 3). Small bodies of gabbro and sagvandite (metasomatic carbonate-orthopyroxenite) occur within the nappe (Schreyer et al., 1972; Lindstrøm and Andresen, 1992). Granulite facies metamorphic conditions at Heia (Fig. 1b) were estimated at 715 ± 30 °C and 9.2 ± 1 kbar using multiple geothermometers and geobarometers (Elvevold, 1987). U-Pb zircon ages from the rocks at Heia indicate high-temperature metamorphism at 439 ± 1 Ma and gabbro crystallization at 435 ± 1 Ma, overprinted by Caledonian shearing at 420 ± 4 Ma (Augland et al., 2014). Greenschist facies mylonitic rocks mark the boundary between the Nordmannvik Nappe and Lyngsfjellet Nappe above. The Lyngsfjellet Nappe is comprised of greenschist to amphibolite facies fossiliferous metasedimentary rocks unconformably overlying the mafic–ultramafic Lyngen Magmatic Complex, interpreted as an ophiolite formed in an incipient arc setting in the Early Ordovician (possible Laurentian arc; Figs. 1, 3; Andresen and Bergh, 1985; Zwaan, 1988; Stephens and Gee, 1989; Andresen and Steltenpohl, 1994; Kvassnes et al., 2004; Augland et al., 2014). Timing and kinematics of emplacement of the Lyngsfjellet Nappe over the Nordmannvik Nappe are unclear.

3 Field results

We investigated the RNC east and north of Lyngen in coastal areas, where it is exposed around a window of KNC rocks (Figs. 1, 2). Detailed structural sections through the RNC were investigated on Uløya, supplemented by structural mapping along the east coast of Lyngen, on Kågen and around Straumfjord, and through the nappe stack on Arnøya (Figs. 2, 3). The nappes on Arnøya were previously assigned to the KNC (Roberts, 1973; Zwaan, 1988), but later reconsidered as being part of the Vaddas Nappe (Andresen, 1988). More recent maps have classified northern Arnøya as part of the Magerøy or Vaddas Nappe and southern Arnøya as KNC (e.g. Corfu et al., 2007; Augland et al., 2014; Gasser et al., 2015). Our own field observations indicate that all three RNC nappes (Vaddas, Kåfjord, and Nordmannvik) are present on Arnøya (Figs. 1b, 2, 3).

3.1 Lithologies

The lower boundary of the RNC towards the KNC was investigated on Uløya and Arnøya (Fig. 2). The underlying KNC comprises either quartzofeldspathic rocks or metapelitic paragneisses (Figs. 3, 4a), whereas the boundary itself consists of a ~ 40 m thick strongly mylonitized zone comprising intercalated amphibolite facies quartzofeldspathic rocks, gneisses, and schists (Fig. 4b). Marbles are locally present together with the amphibolite and schist. On Uløya, a migmatitic paragneiss that forms part of the KNC below the boundary is subsequently mylonitized in the solid state, with centimetre-sized porphyroclasts of garnet and feldspar (Fig. 4b, c). Kinematic indicators consistently show top-to-SE shearing. Above the mylonitic layer, sheared metaconglomerate (Fig. 4d) occurs together with a marble unit, which marks the base of the Vaddas Nappe on Arnøya, Kågen, and Uløya (Fig. 3). This marble layer is overlain by amphibolite and calc-schist (Fig. 4e). Two main marble units are found in the Vaddas Nappe at Straumfjord: one in the lower Vaddas and one in the upper Vaddas (Fig. 3). The marble at the

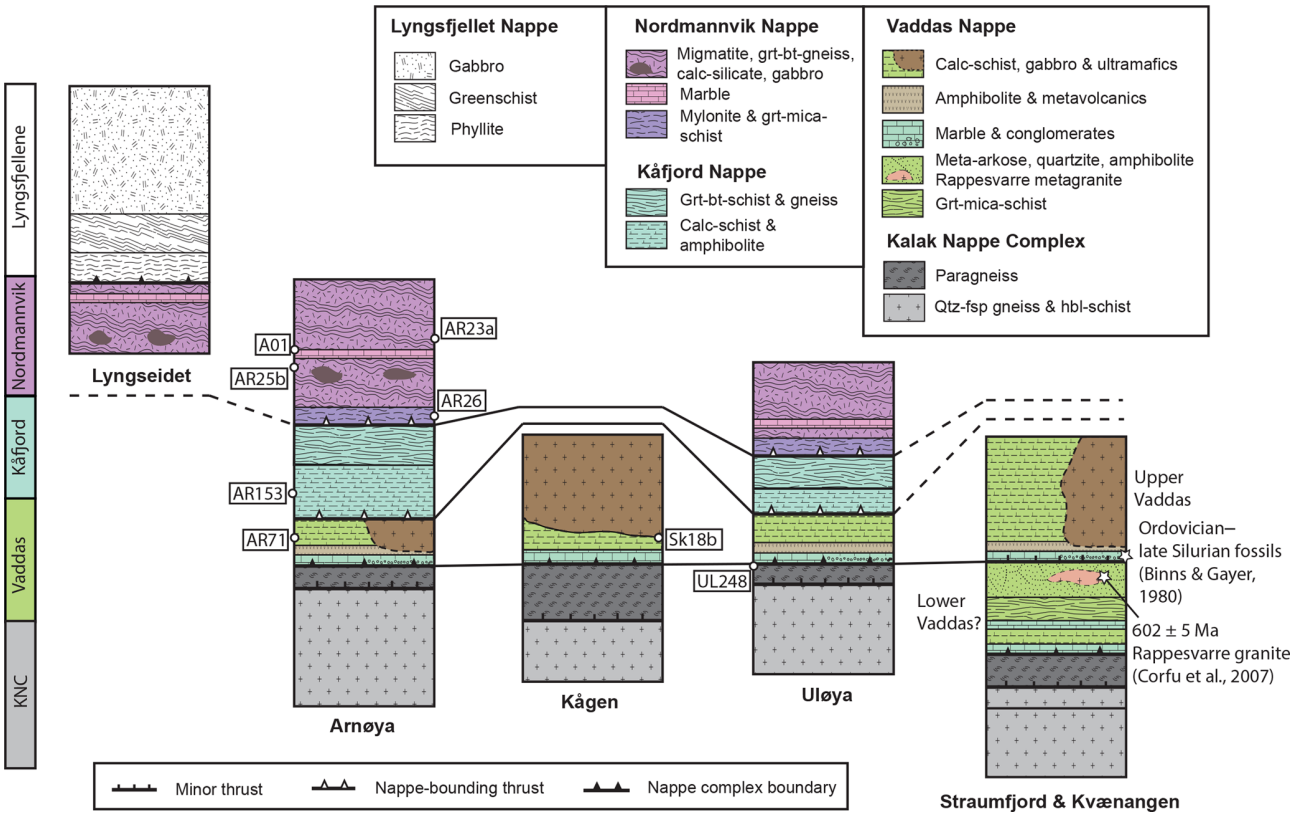

Figure 3. Representative tectonostratigraphy of the RNC from Lyngseidet (west) to Straumfjord and Kvænangen (east) showing the location of major structures and relative thickness and spatial variation in tectonic units. Based on Zwaan (1988), Lindahl et al. (2005), and own work. The tectonostratigraphic position of the investigated samples is indicated.

base of the lower Vaddas is variably sheared and overlain by intercalated metasediments and metapsammites similar to those in the KNC. The upper marble layer marks the base of the upper Vaddas and is associated with sheared conglomerates. It is overlain by amphibolite and calc-schist, similar to the Vaddas succession on Arnøya, Kågen, and Uløya, and we consider that only the upper Vaddas is found on these three islands (Fig. 3). On Arnøya, Kågen, and in Straumfjord, gabbro intrusions in the upper Vaddas Nappe (Figs. 2, 3) are associated with local migmatization of the surrounding metasediments, showing a clear intrusive relationship.

A well developed strongly mylonitic foliation in muscovite-rich garnet-mica-schist marks the Vaddas–Kåfjord nappe boundary on Uløya and Arnøya (Figs. 2, 3). The boundary cuts a gabbro body in the Vaddas Nappe on Arnøya (Fig. 3). The Kåfjord Nappe is comprised of a lower unit of homogenous garnet-mica-zoisite-schist with calc-silicate lenses and some amphibolite layers (Fig. 4g–i), and a homogenous upper unit comprised of garnet-mica-schist and gneiss. This upper unit often displays strongly sheared layers rich in quartz-feldspar sigma clasts, possibly indicating the presence of leucosome prior to mylonitization. The lower Kåfjord is similar to the calc-schists in the underlying Vaddas Nappe, whereas the upper Kåfjord is similar to strongly sheared rocks in the Nordmannvik Nappe (e.g. Figs. 3, 5a). Both units are pervasively and strongly sheared at amphibolite facies conditions. The Kåfjord–Nordmannvik boundary consists of mylonitic gneisses and garnet-mica-schist at least 50 m thick. The Nordmannvik Nappe is mainly comprised of garnet-biotite-gneiss with layers and lenses of amphibolite and local calc-silicates, generally dominated by a mylonitic foliation (Fig. 5a, b). Further away from the nappe boundary rare relict lenses (< 50 m) display a higher-grade migmatitic foliation (Fig. 5c). On Arnøya, the frequency of relict lenses increases upwards away from the nappe boundary. The migmatite comprises felsic leucosome and biotite, garnet, and kyanite in the restite. The amount of leucosome varies spatially between 5 % and 25 % (Fig. 5d, e). Layers of amphibolite in the nappe also contain minor tonalitic leucosome suggesting that the mafic rocks have also been migmatized.

3.2 Structures

The earliest observed structural element is the syn-migmatitic foliation observed in the low-strain lenses in the Nordmannvik Nappe (S_1; Figs. 2a, e, 5c–e). In most cases it is sheared and overprinted by the solid-state amphibolite-

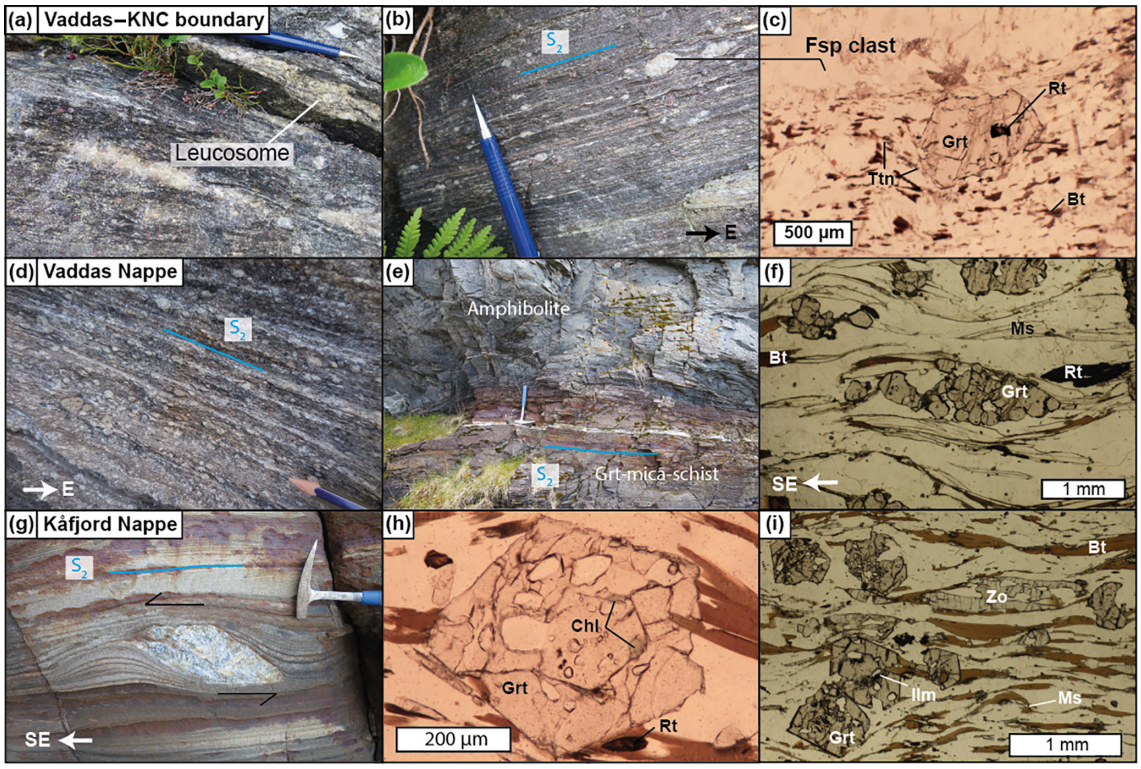

Figure 4. Field photographs and photomicrographs from Vaddas and Kåfjord nappes. Coordinates for sample sites are given in Table 1. **(a)** KNC paragneiss with visible (sheared) leucosome from 30 m below the Vaddas–KNC boundary shear zone at site UL248. **(b)** The Vaddas–KNC boundary mylonite at site UL248. **(c)** Photomicrograph of sample UL248 showing the edge of a K-feldspar porphyroclast, garnet with a rutile inclusion, and matrix with biotite and titanite visible. **(d)** Sheared metaconglomerate from the base of the Vaddas Nappe on Uløya at lat 69.89326, long 20.55713 with mostly rounded quartzite clasts in a pelitic matrix of biotite and garnet. **(e)** Typical strongly sheared garnet-mica-schist and amphibolite sample in the Vaddas Nappe at lat 69.89326, long 20.55456 (Uløya). **(f)** Photomicrograph of Vaddas Nappe sample AR71 showing sheared garnet (top-to-SE shear sense), and muscovite fish, biotite, and rutile in the matrix. **(g)** An outcrop of a sheared calc-silicate lens (top-to-SE shear sense) in a typical garnet-zoisite-biotite schist from the lower Kåfjord Nappe at lat 69.85701, long 20.53317. **(h)** Photomicrograph of garnet in Kåfjord Nappe sample AR153 showing distinctive core and rim structure with chlorite inclusions in garnet cores and rutile in the matrix. **(i)** Photomicrograph of Kåfjord Nappe sample AR153 showing garnet porphyblasts in a matrix with S_2 foliation defined by zoisite, biotite, and muscovite. An ilmenite inclusion in garnet is also shown.

facies S_2 mylonitic foliation, which is pervasive throughout all the nappes of the RNC and underlying KNC (Fig. 2a–f). In the lower strain lenses the S_1 migmatitic foliation is found in three structural orientations: (1) as a steep foliation that shows a variable trend (rare; Fig. 5c); (2) folded in open to closed folds with axial planes (containing leucosome) parallel to the S_2 foliation (Fig. 5d); and (3) most commonly as a shallowly dipping foliation, parallel to the S_2 foliation (Fig. 2a, d, e). Fold hinges in the migmatites (F_2) plunge towards the SE or NW, parallel to the L_2 stretching lineation. An L_2 intersection lineation between S_1 and S_2 is observed in the Nordmannvik and upper Kåfjord nappes. On Arnøya it is mostly parallel to the L_2 stretching lineation, whereas on Uløya it also plunges shallowly towards the SW and W as well, consistent with the presence of a variable S_1 foliation in the upper Kåfjord Nappe (Fig. 2a, d, e).

The amphibolite-facies solid-state S_2 foliation is generally flat-lying, dipping slightly to the west or north-west in the northern and western parts of the area, and toward the east and south-east in the eastern part of the field area. The main variation is around the larger gabbro bodies, where the S_2 foliation is deflected around them (Fig. 2). Gabbro interiors are nearly unaffected by S_2 shearing, with most of the deformation confined along their boundaries. The S_2 foliation is associated with a generally NW–SE-trending stretching lineation (L_2; Fig. 2) and always top-to-SE shear sense indicators (Fig. 4b, f, g). In the Vaddas and lower Kåfjord metasediments local micro- to meso-scale isoclinal folds transpose a pre-S_2 foliation. Dismembered fold hinges are common, with fold axes normally parallel to the L_2 stretching lineation and axial planes parallel to S_2 (Fig. 2a, b, d, e). The KNC–Vaddas, Vaddas–Kåfjord, and Kåfjord–Nordmannvik nappe boundaries generally display a relatively stronger S_2 mylonitic foliation than within the nappes, and the L_2 stretching lineation at the nappe boundaries is often more pronounced than within nappe interiors. We associate S_1 in the RNC with

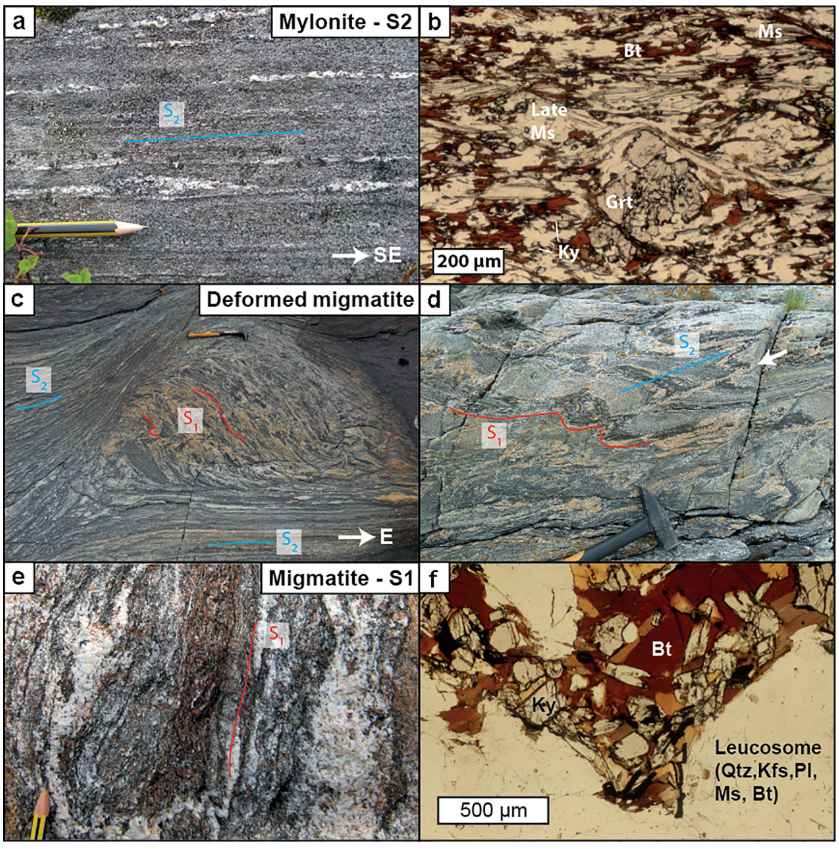

Figure 5. Field photographs and photomicrographs from the Nordmannvik Nappe. **(a)** Nordmannvik mylonite (solid-state deformed, S_2, migmatite) at sample site AR26 near the Nordmannvik–Kåfjord boundary. **(b)** Photomicrograph of sample AR26 showing garnet porphyroblasts with sillimanite inclusions in a matrix and a strong S_2 foliation defined by biotite, kyanite, and muscovite. **(c)** A lens-shaped domain in the Nordmannvik Nappe on Uløya at lat 69.84046, long 20.51852 with an older S_1 migmatitic foliation overprinted and sheared by solid-state S_2 mylonitic foliation. **(d)** Nordmannvik migmatite at site AR23 showing the folded S_1 migmatitic foliation (Caledonian fold geometry) with a melt segregation in an axial planar orientation (white arrow; parallel to S_2). **(e)** Nordmannvik migmatite at sample site AR25b showing a high volume of leucosome and garnet- and biotite-rich melanosomes. **(f)** Photomicrograph of sample AR25b showing a lack of S_2 foliation, and kyanite and biotite along the edge of a leucosome segregation.

D_1 and S_2, and L_2 with D_2. The S_1 in the KNC may be older than the S_1 in the RNC (pre-D_1).

3.3 Tectonostratigraphic interpretation

Based on our field observations we propose a correlation of the different parts of the RNC across the study area (Fig. 3). Lithological similarities indicate that the basal marble and conglomerate layer of the Vaddas Nappe on Arnøya, Kågen, and Uløya correlates with the uppermost marble and conglomerate layer at the base of the upper Vaddas Nappe around Straumfjord at a similar tectonostratigraphic level to where Binns and Gayer (1980) identified early Silurian fossils (Fig. 3). This indicates that the lower Vaddas rocks, which are relatively thick in the eastern study area, thin out towards the north and west and are not present elsewhere in the field area (Fig. 3). The lower Vaddas unit includes the Rappesvarre granite, and, based on the structural and lithological similarity to the underlying KNC, we favour the interpretation that it is either a composite nappe of KNC and upper Vaddas rocks, or reworked KNC rocks, as suggested by Corfu et al. (2007) and Gee et al. (2017). More work needs to be done to establish whether it has more RNC or KNC affinity (perhaps Corrovarre Nappe) to constrain its extent south of the field area.

Gabbros are characteristic of the upper Vaddas Nappe, and the continuation of the Kågen gabbro on southern Arnøya indicates that the upper Vaddas Nappe is present there as well (Figs. 2, 3). Our investigation on Arnøya shows an identical nappe stack as present on Uløya, indicating that the north-western half of Arnøya is part of the RNC, including the upper Vaddas, Kåfjord, and Nordmannvik nappes (Figs. 2, 3). The kyanite-bearing migmatites and gneisses on the northern part of Arnøya are assigned to the Nordmannvik Nappe based on their similarity to migmatites at Lyngseidet and on southern Uløya, and their tectonostrati-

graphic position (Fig. 3). We separate the Kåfjord Nappe, based on lithological differences, into upper and lower parts. The upper part is similar to the strongly sheared rocks of the Nordmannvik Nappe, and records a Rb-Sr whole-rock age of ∼ 440 Ma age, possibly for anatexis (Dangla et al., 1978). It could alternatively be considered as part of the Nordmannvik Nappe. The lower part consists of calcareous metasediments that show no evidence of prior anatexis and are more similar to the underlying metasediments of the Vaddas Nappe. Although the lower part of the Kåfjord Nappe in the field area is comprised of similar metasediments to the Vaddas Nappe (suggesting they may be related), it is defined as its own nappe because its base cuts the upper part of the gabbro in the Vaddas Nappe on Arnøya. All nappes show significant thickness variations, which are partly due to the undeformed Kågen and Kvænangen gabbros that are large boudins. Erosion has removed all units above them, e.g. the Kåfjord and Nordmannvik nappes (Fig. 3). The entire Vaddas Nappe, as it is currently defined, shows a thickness of 100–1500 m with its lower part wedging out towards the west and north. The Kåfjord Nappe is thickest in its southern part (> 1000 m) and thins towards Arnøya (< 1000 m), whereas the Nordmannvik Nappe is much thicker (> 2000 m) than the Vaddas or Kåfjord nappes and thickest on Arnøya (Figs. 2, 3). This results in flat-lying laterally extensive but lensoid thrust sheets, which are separated by mylonitic shear zones but which are internally pervasively sheared (Fig. 2).

4 Metamorphism in the RNC

Metamorphic conditions were investigated throughout the entire RNC in order to resolve variations in pressure and temperature (P–T), and deformation conditions throughout the nappe stack. Sample sites and details are shown in Figs. 2, 3, and Table 1. Table 2 gives a summary of the mineralogy in the samples used for P–T modelling. Mineral abbreviations are according to Whitney and Evans (2010).

4.1 Methods

P–T conditions for all samples were estimated using phase equilibrium modelling with the Perple_X software (Connolly, 2005: version 6.6.6) using the internally consistent thermodynamic dataset of Holland and Powell (1998).

The calculations were performed in the MnNCKFMASHTi system using X-ray fluorescence (XRF) whole-rock compositions (Table S1 in the Supplement). The following solution mixing models were used: garnet, staurolite, chloritoid (Holland and Powell, 1998), biotite (Tajčmanová et al., 2009), ternary feldspar (Fuhrman and Lindsley, 1988), ilmenite (ideal mixing of ilmenite, geikielite, and pyrophanite endmembers), melt (Holland and Powell, 2001), and white mica (Coggon and Holland, 2002). Iron was assumed to be Fe^{2+} as the Fe^{3+} content of the minerals considered is negligible and Fe^{3+} oxides occur in negligible amounts. Apatite was observed in all samples and therefore the corresponding amount of CaO bonded to P_2O_5 observed in the whole-rock analyses was subtracted from the bulk compositions. Measured chemical compositions of the relevant minerals (Tables 3 and 4) were compared with model isopleths in the calculated pseudosections. Molar percent of grossular (Grs) and spessartine (Sps) endmembers and the X_{Mg} ($Mg/Mg + Fe_{tot}$) value in garnet are used to constrain P–T conditions, and are shown on the P–T sections. Estimated P–T conditions were checked with anorthite content in plagioclase (An=Ca/(Ca + Na + K)), X_{Mg} ($Mg/(Mg + Mn + Fe_{tot})$) in biotite, and Si content in white mica, and are shown on some pseudosections where they assist with further constraining P–T estimates. Fluid content was derived from the loss on ignition (LOI) values unless stated otherwise, and considered as pure H_2O in all calculations.

4.2 Kalak–Vaddas boundary (UL248)

4.2.1 Petrography and mineral chemistry

Sample UL248 (Figs. 2, 3, 4b; Table 1) represents a mylonitized migmatitic paragneiss from the upper part of the KNC (Fig. 4a, b). The fine-grained matrix of sample UL248 contains porphyroblasts of garnet (up to 0.9 mm) and fragments (up to 5 mm) of plagioclase, K-feldspar, and quartz-feldspar aggregates (Fig. 4c). Biotite, muscovite, and elongate grains and aggregates of quartz and feldspar define the S_2 mylonitic foliation. Two generations of muscovite are found as (1) rare large (0.2 mm) mica fish parallel to the S_2 foliation (Ms_1), and (2) as small grains intergrown with biotite and along garnet and K-feldspar boundaries, within the S_2 foliation (Ms_2). Quartz, biotite, and rutile are common as inclusions in garnet (Fig. 4c). Minor rutile is also found in the matrix. Titanite is abundant as elongate, 0.02–0.35 mm long, grains parallel to the S_2 foliation and as inclusions in garnet rims (Figs. 4c, 6a). Distinctive garnet zoning displays two generations of garnet. Garnet cores (Grt_1) have a relatively flat compositional profile, followed by a transition zone to a ∼ 0.1–0.15 mm thick rim (Grt_2; Fig. 6a). The two generations show significantly different compositions. Grt_1 is lower in Grs (Grs_{10-12}), higher in spessartine (Sps_{12-15}), and has a higher X_{Mg} content (0.11–0.13) than Grt_2. The latter displays the following composition: Grs_{36-38}, Sps_{3-4}, and X_{Mg} content of 0.08–0.11. Grt_2 (rims) grew together with biotite, titanite, plagioclase (rims), and Ms_2 during top-to-SE S_2-associated shearing. X_{Mg} in biotite ranges between 0.36 and 0.45. Plagioclase generally shows zoning with a higher anorthite content in the cores (An_{25-28}) than in rims (An_{20-23}). Early muscovite (Ms_1) has a Si content of 3.06–3.08 (a.p.f.u., atoms per formula unit), whereas later muscovite (Ms_2) associated with the S_2 foliation has a higher Si content of 3.20–3.27 (a.p.f.u.; Table 4). The relict compositions shown by

Table 1. List of samples with rock types, sample sites, and methods.

Sample	Nappe	Rock type	Sample site (lat, long)	Method	Context
UL248	Kalak–Vaddas	Grt-bt-mylonite	69.86755, 20.60304	*P–T* modelling, U-Pb titanite	lower part of ∼ 40 m thick mylonite zone
AR71	Vaddas	Grt-micaschist	70.06315, 20.45522	*P–T* modelling	upper ∼ 30 m of ∼ 120 m thick Vaddas Nappe
Sk18b	Vaddas	gabbroic pegmatite	69.985900, 20.829567	U-Pb zircon	pegmatite near the edge of Kågen gabbro
AR153	Kåfjord	Grt-bt-zo-schist	70.06797, 20.44341	*P–T* modelling	mid- to lower-Kåfjord Nappe
AR23a	Nordmannvik	pelitic migmatite	70.205343, 20.522562	U-Pb zircon	lens with S1 foliation
AR25b	Nordmannvik	pelitic migmatite	70.16425, 20.52112	*P–T* modelling	lens with S1 foliation
AR26	Nordmannvik	Grt-bt-ky-schist	70.137455, 20.561118	*P–T* modelling	mylonite ∼ 50 m above Nordmannvik–Kåfjord boundary (S_2 foliation)
A01	Nordmannvik	Calc-silicate	70.191422, 20.503611	U-Pb titanite	S1 lens, interaction zone between calc-silicate layers and leucosome

Table 2. Mineralogy for petrology samples.

		Main minerals										Accessory minerals						
Nappe	Sample	Bt	Pl	Qtz	Grt	Kfs	Sil	Ky	Zo	Ms	Chl	Zrn	Mnz	Rt	Ttn	Ill	Ap	Ep/All
Kalak–Vaddas	UL248	×	×	×	×	×				×		×		×	×	×	×	×
Vaddas	AR71	×	×	×	×					×		×		×		×	×	
Kåfjord	AR153	×	×	×	×				×	×	Gt in.	×		×	×	×	×	
Nordmannvik	AR25b	×	×	×	×	×	×	×		×		×	×			×	×	
Nordmannvik	AR26	×	×	×	×		Gt in.	×		×		×				×	×	

Grt_1, plagioclase cores, and large Ms_1 fish indicate that pre-D_2 *P–T* conditions may be preserved in this sample.

4.2.2 *P–T* modelling

Garnet cores represent an earlier *P–T* history, shielded from re-equilibration with the matrix by garnet rims during subsequent metamorphism, and the conditions for garnet core and rim formation were therefore modelled separately. Garnet core formation was modelled using the composition obtained from the bulk rock XRF analysis (Table S1). Since leucosome was observed in less sheared outcrops of the same rock type within 10 m of the sample site, garnet cores in the sample were modelled as part of a migmatite assemblage. The pressure was estimated to be 10 kbar based on the position of garnet isopleths representing measured garnet core compositions in a water-saturated pseudosection. The water content was then estimated from the position of the solidus in a *T*–X_{H_2O} pseudosection calculated at 10 kbar. In Fig. 7a modelled X_{Mg}, Grs, and Sps compositions fit measured garnet core compositions within the phase field Grt-Bt-Pl-Kfs-Ms-Rt-Qtz-Melt, constraining pre-D_2 conditions between 705–735 °C and 9.9–10.8 kbar. As diffusion in garnet at upper amphibolite facies conditions is considered to be fast (e.g. Caddick et al., 2010), care should be taken with interpreting these as absolute *P–T* conditions as garnet cores could have been modified by diffusion during the overprinting event. However, we interpret the shape of the garnet profile to indicate that diffusion is reflected by the transition zone between Grt_1 cores and Grt_2 rims, and that the flat cores probably represent Grt_1 that escaped diffusion during formation of the S_2 foliation (Fig. 6a). The interpretation is consistent with the presence of rutile and lack of titanite as inclusions in garnet cores (Figs. 4c, 6a). It also agrees well with the anorthite (An_{25-29}) content in zoned plagioclase cores and Si content of large Ms_1 mica fish (Table 4).

The *P–T* estimate for formation of garnet rims and the S_2 foliation (Fig. 7b) was calculated with the XRF bulk rock composition from which garnet cores were subtracted by using the modal Grt_1 proportion estimated from the pseudosection (0.75 modal %). LOI from the bulk rock analysis was used as H_2O content. Modelled X_{Mg}, Sps, and Grs compositions fit measured garnet rim compositions in the phase field Grt-Bt-Ms-Pl-Kfs-Ttn-Rt-Qtz, and constrain formation of the S_2 foliation between 635 and 690 °C and between 11.5 and 12.3 kbar (Fig. 7b). Anorthite content in plagioclase

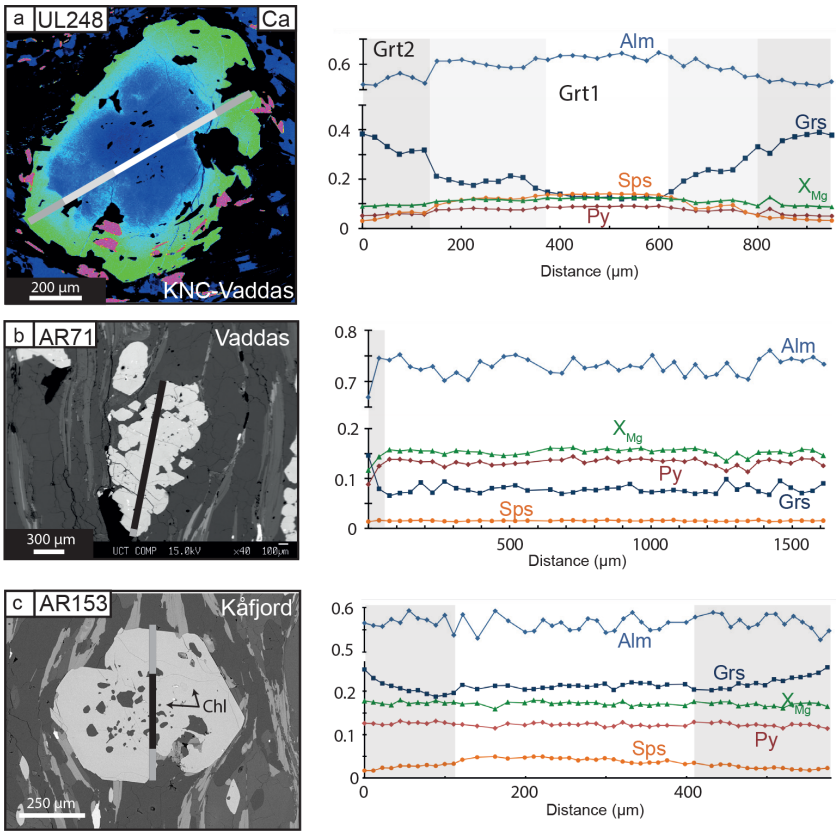

Figure 6. Backscattered electron (BSE) images, compositional maps, and garnet profiles from the Vaddas and Kåfjord nappes. **(a)** Garnet from the KNC–Vaddas boundary, sample UL248, displays strong zoning with defined core (Grt1) and rim (Grt2) zones and a transition zone between them. Pink grains in garnet rims are titanite. **(b)** Garnet from the Vaddas Nappe, sample AR71, has a flat profile with occasional thin growth rims. **(c)** Garnet from the Kåfjord Nappe, sample AR153, has a profile that shows some zoning, with mainly Grs and Sps contents displaying a difference between inclusion-rich cores and inclusion-poor rims.

rims, X_{Mg} content in matrix biotite, and Si content of Ms_2 agree well with this estimate. Titanite is predicted as part of this assemblage, which is consistent with the large amount of titanite in the matrix and as inclusions in Grt_2 (Figs. 4c, 6a). Based on field structural observations we interpret this P–T estimate for S_2 to represent shearing along the KNC–Vaddas boundary, and titanite growth is directly related to this event.

4.3 Upper Vaddas Nappe (AR71)

4.3.1 Petrography and mineral chemistry

Sample AR71 (Figs. 2, 3; Table 1) is a medium-grained garnet-mica-schist with a strong S_2 foliation defined by intergrown biotite and muscovite (Fig. 4f). Muscovite is the dominant mica and occurs as large (1–3 mm long) mica fish. Plagioclase is found as rare porphyroclasts and as single recrystallized grains within quartz layers. Rutile is abundant as elongate grains parallel to the foliation (Fig. 4f). Minor ilmenite occurs as rims on rutile grains. Garnet grains are found as small (0.03–0.1 mm), single, idiomorphic grains and as larger (1–2 mm) fish-shaped clusters of grains parallel to the foliation, with a synkinematic geometry displaying a typical Caledonian top-to-SE shear sense (Fig. 4f). Garnet shows an almost flat compositional profile with slight variations between cores, intermediate zones, and rims. In rare cases fish-shaped garnets have a thin rim of a different composition. These rims only occur at the apex of fish-shaped garnets and are never present on the S_2 parallel rims, indicating that they represent growth of garnet during late D_2 shearing (e.g. Fig. 6b, Table 3). In garnets that do not display the thin rim, X_{Mg} varies from 0.17 in the cores to 0.14 in the intermediate zones and garnet edges. Grs is slightly lower in cores (Grs_{7-8}) than intermediate zones and edges (Grs_{9-10}). Sps content varies between 1.4 and 1.6 mol %. Almandine content varies between 68 and 73 mol % (Fig. 6b, Table 3). The thin garnet rims display the following composition: Alm_{65-67} Grs_{14-16} $Sps_{1.2}$ and an X_{Mg} of ~ 0.11 (e.g. Fig. 6b, Table 3). X_{Mg} in biotite ranges between 0.50 and 0.53, Si content in muscovite is between 3.05 and 3.11 (a.p.f.u.), and plagioclase has an anorthite content of 18–20 mol % (Table 4).

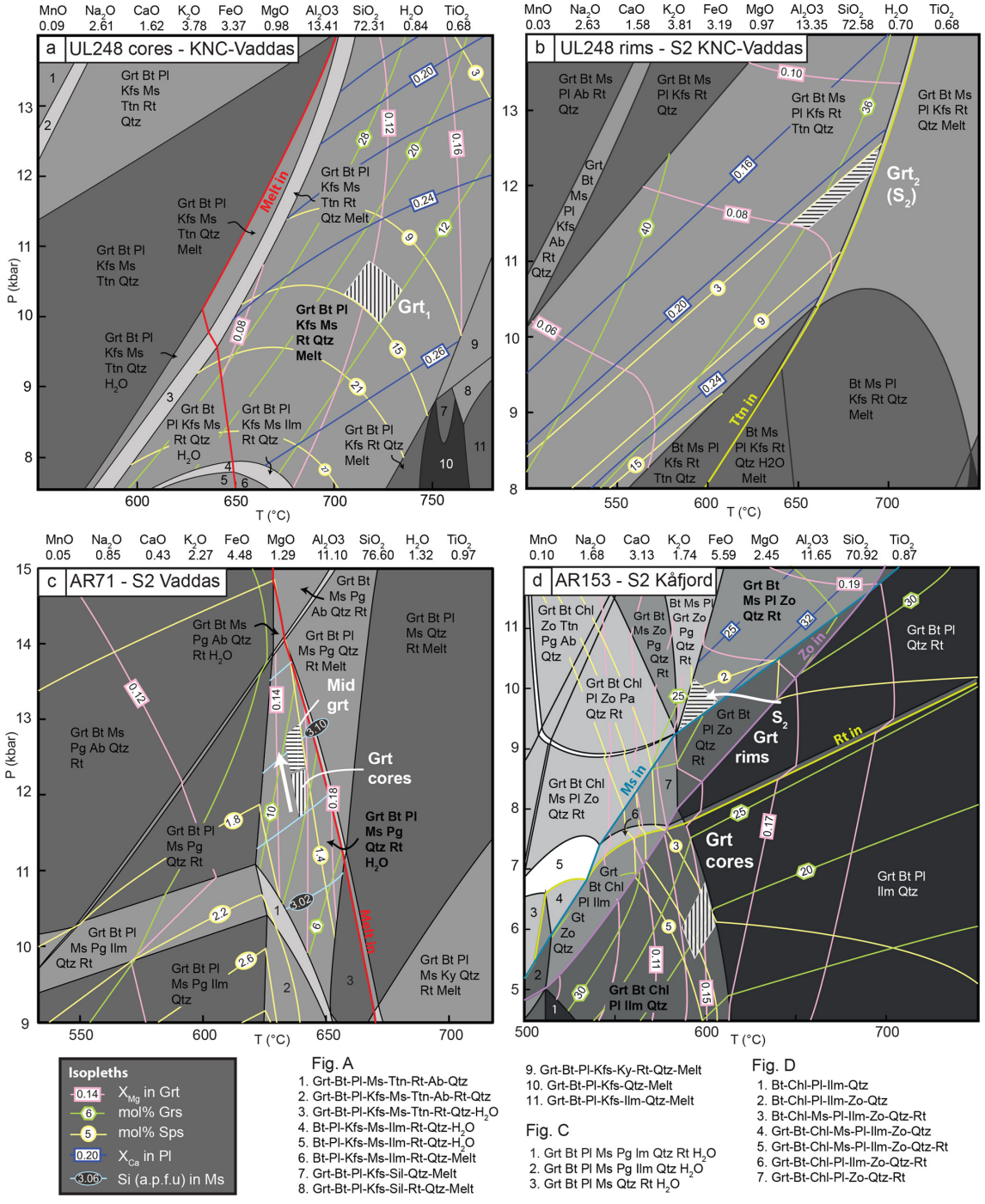

Figure 7. Pseudosections describing metamorphism at the Kalak–Vaddas nappe boundary (sample UL248) and in the Vaddas (sample AR71) and Kåfjord (sample AR153). Estimates in the pseudosections are displayed as striped boxes. **(a)** Garnet core (Grt_1) growth conditions were estimated from the X_{Mg}, Grs, and Sps contents of garnet cores. Isopleths for anorthite content are shown, and are in agreement with measured anorthite content in plagioclase cores. The pseudosection was calculated using the bulk composition determined from XRF analysis of the whole rock. **(b)** S_2 foliation conditions were estimated from X_{Mg}, Grs, and Sps content correlating with measured garnet rims (Grt_2). The estimate correlates well with anorthite content in plagioclase rims. The pseudosection was calculated using a bulk composition from which garnet cores were subtracted. **(c)** Grs, Sps, and X_{Mg} contents in garnet give core and rim at slightly lower and higher pressures, respectively. Si (a.p.f.u) in muscovite was used to further constrain pressures. **(d)** Grs, Sps, and X_{Mg} contents in zoned garnets from the Kåfjord Nappe give a garnet core estimate at lower pressure conditions, and garnet rim estimate at higher pressure conditions. Chlorite and ilmenite inclusions in garnet cores are consistent with the garnet core estimate.

Table 3. Representative garnet analyses showing recalculated garnet compositions on the basis of 8 cations and 12 oxygens.

	Grt																			
Nappe	Kalak–Vaddas boundary				Vaddas				Kåfjord				Nordmannvik (migmatite)				Nordmannvik (mylonite)			
Sample	UL248				AR71				AR153				AR25b				AR26			
	Core (Grt1)	Rim (Grt2)	Core (Grt1)	Rim (Grt2)	Core	Rim (late)	Core	Rim	Core	Rim	Core	Rim	Core	Rim	Core	Rim (lrg)	Grt core (lrg)	Grt rim (sml)	Grt core (sml)	Grt rim
wt %							*	*					*	*	*	*	*	*	*	*
SiO_2	37.63	38.01	37.47	38.00	37.74	37.76	37.72	37.58	37.81	37.60	37.60	37.59	38.61	38.14	37.87	37.59	37.76	37.67	37.72	37.91
TiO_2	0.00	0.07	0.00	0.08	0.07	0.04	0.00	0.00	0.13	0.05	0.01	0.05	0.03	0.04	0.00	0.00	0.01	0.03	0.01	0.03
Al_2O_3	21.64	21.41	21.49	21.46	21.81	21.82	22.00	21.77	21.94	22.51	22.05	22.57	22.00	21.92	21.89	21.64	21.67	21.60	21.76	21.56
Fe_2O_3	0.00	0.63	0.00	0.00	0.00	0.00	0.00	0.00	0.00	0.00	0.00	0.00	0.00	0.00	0.00	0.00	0.00	0.00	0.00	0.00
FeO	28.74	24.13	29.33	24.01	33.44	31.45	32.71	33.26	27.08	26.12	28.03	27.25	30.13	31.28	31.35	31.21	33.77	34.26	32.25	33.00
MnO	6.25	1.66	6.06	1.76	0.69	0.63	0.64	0.70	1.54	0.80	1.55	0.86	1.44	1.61	1.62	1.63	0.49	0.52	1.53	1.58
MgO	2.24	1.38	2.28	1.32	3.48	2.32	3.54	3.18	3.06	3.25	3.13	3.09	5.90	4.63	5.32	4.85	4.53	4.08	4.54	3.53
CaO	4.52	13.46	4.02	13.38	2.73	5.35	2.62	3.19	7.91	8.79	6.89	8.04	1.70	2.07	2.06	2.50	1.56	1.68	2.11	2.18
Total	101.02	100.75	100.65	100.01	99.96	99.37	99.23	99.68	99.47	99.12	99.26	99.45	99.81	99.69	100.11	99.42	99.79	99.84	99.92	99.79
Si	2.991	2.986	2.993	3.003	3.011	3.034	3.029	3.008	3.001	2.978	2.995	2.972	3.030	3.032	2.988	2.993	3.009	3.010	2.998	3.013
Ti	0.000	0.004	0.000	0.004	0.004	0.002	0.000	0.000	0.008	0.003	0.001	0.003	0.002	0.002	0.000	0.000	0.001	0.002	0.001	0.002
Al	2.028	1.983	2.023	1.999	2.051	2.067	2.082	2.054	2.053	2.101	2.070	2.103	2.042	2.054	2.036	2.031	2.036	2.034	2.038	2.023
Fe^{3+}	0.000	0.037	0.000	0.000	0.000	0.000	0.000	0.000	0.000	0.000	0.000	0.000	0.000	0.000	0.000	0.000	0.000	0.000	0.000	0.000
Fe^{2+}	1.910	1.585	1.959	1.587	2.231	2.113	2.196	2.226	1.797	1.730	1.867	1.801	1.984	2.079	2.068	2.078	2.250	2.289	2.143	2.205
Mn	0.421	0.110	0.410	0.118	0.046	0.043	0.044	0.047	0.104	0.054	0.105	0.058	0.096	0.108	0.108	0.110	0.033	0.035	0.103	0.100
Mg	0.265	0.161	0.271	0.155	0.414	0.278	0.424	0.379	0.362	0.384	0.372	0.364	0.692	0.549	0.626	0.576	0.538	0.486	0.538	0.468
Ca	0.385	1.133	0.344	1.133	0.233	0.461	0.225	0.274	0.673	0.746	0.588	0.681	0.143	0.176	0.174	0.213	0.133	0.144	0.180	0.188
X_{alm}	0.641	0.530	0.656	0.530	0.763	0.730	0.703	0.734	0.592	0.575	0.622	0.599	0.623	0.661	0.689	0.693	0.740	0.751	0.714	0.698
X_{prp}	0.089	0.054	0.091	0.052	0.142	0.096	0.136	0.125	0.119	0.127	0.124	0.121	0.217	0.174	0.209	0.192	0.177	0.159	0.179	0.153
X_{sps}	0.141	0.037	0.137	0.039	0.016	0.015	0.014	0.016	0.034	0.018	0.035	0.019	0.030	0.034	0.036	0.037	0.011	0.012	0.034	0.033
X_{grs}	0.129	0.379	0.115	0.379	0.080	0.159	0.072	0.090	0.221	0.248	0.196	0.226	0.045	0.056	0.058	0.071	0.044	0.047	0.060	0.061
X_{Mg}	0.122	0.092	0.122	0.089	0.156	0.116	0.162	0.146	0.168	0.182	0.166	0.168	0.259	0.209	0.232	0.217	0.193	0.175	0.201	0.175

* Energy dispersive X-ray spectroscopy (EDS) scanning electron microscope (SEM) analyses.

Table 4. Representative biotite, feldspar and white mica compositions.

Sample	Muscovite						Biotite									Plagioclase						
	UL248		AR71	AR153	AR26	AR25b	UL248		AR71	AR153		AR26			AR25b	UL248		AR71	AR153	AR26	AR25b	
	Early	Late				Late	Grt in.	Mtx		Early	Late	Grt in.	Mtx	Rest	Leuco	Core	Rim				Rest	Leuco
wt %																						
SiO_2	46.32	48.26	46.69	48.33	45.72	45.31	36.79	36.29	36.98	38.06	38.26	37.82	36.18	36.04	36.05	61.17	62.75	64.92	60.48	63.01	61.51	61.79
TiO_2	1.08	1.00	0.84	0.94	1.27	1.79	3.53	2.95	2.33	1.93	0.78	3.58	4.58	3.84	3.67	0.00	0.00	0.00	0.00	0.00	0.02	0.01
Cr_2O_3	0.03	0.03	0.02	0.02	0.04	0.05	0.01	0.01	0.05	0.10	0.03	0.00	0.00	0.11	0.02	0.00	0.00	0.00	0.00	0.00	0.00	0.00
Al_2O_3	33.27	30.78	34.06	32.99	34.67	34.24	17.33	16.94	18.57	20.60	19.53	20.57	17.69	18.74	19.36	23.95	23.01	23.27	25.40	23.34	24.60	24.95
Fe_2O_3	2.15	0.84	0.00	0.00	0.00	1.26	0.00	0.00	0.00	0.00	0.00	0.00	0.00	0.00	0.00	0.04	0.20	0.00	0.01	0.00	0.00	0.00
FeO	0.47	1.83	1.40	1.63	1.06	0.27	21.55	21.26	19.44	15.98	16.50	13.80	18.48	17.95	17.52	0.00	0.00	0.00	0.00	0.06	0.00	0.04
MnO	0.02	0.05	0.02	0.00	0.00	0.00	0.23	0.22	0.05	0.05	0.04	0.01	0.00	0.04	0.06	0.00	0.00	0.00	0.05	0.03	0.06	0.03
MgO	1.09	1.76	1.44	1.61	1.07	1.16	6.82	7.81	11.46	11.69	13.59	11.62	9.13	11.45	10.33	0.00	0.00	0.01	0.00	0.00	0.00	0.00
CaO	0.00	0.00	0.00	0.00	0.00	0.00	0.02	0.00	0.00	0.00	0.01	0.09	0.00	0.00	0.00	5.48	4.44	3.69	5.59	4.95	5.85	6.16
Na_2O	0.36	0.25	1.11	0.76	0.40	0.34	0.10	0.07	0.22	0.19	0.17	0.00	0.09	0.16	0.11	8.58	9.34	9.18	8.34	8.61	8.16	7.93
K_2O	11.25	11.30	9.46	10.17	10.55	11.14	10.03	10.16	8.17	8.94	9.03	9.09	8.89	10.03	10.18	0.22	0.22	0.05	0.07	0.18	0.28	0.23
Total	96.03	96.10	95.04	96.46	94.77	95.57	96.41	95.70	97.27	97.54	97.93	96.58	95.04	98.36	97.29	99.43	99.96	101.12	99.94	100.18	100.48	101.14
Si	3.09	3.22	3.11	3.19	3.07	3.03	2.91	2.87	2.82	2.86	2.84	2.87	2.86	2.71	2.75	2.73	2.77	2.84	2.68	2.79	2.72	2.72
Ti	0.05	0.05	0.04	0.05	0.06	0.09	0.21	0.18	0.13	0.11	0.04	0.20	0.27	0.22	0.21	0.00	0.00	0.00	0.00	0.00	0.00	0.00
Cr	0.00	0.00	0.00	0.00	0.00	0.00	0.00	0.00	0.00	0.01	0.00	0.00	0.00	0.01	0.00	0.00	0.00	0.00	0.00	0.00	0.00	0.00
Al	2.61	2.42	2.68	2.56	2.74	2.70	1.61	1.58	1.67	1.82	1.71	1.84	1.65	1.66	1.74	1.26	1.20	1.20	1.33	1.22	1.28	1.30
Fe^{3+}	0.11	0.04	0.00	0.00	0.00	0.06	0.00	0.00	0.00	0.00	0.00	0.00	0.00	0.00	0.00	0.00	0.01	0.00	0.00	0.00	0.00	0.00
Fe^{2+}	0.03	0.10	0.08	0.09	0.06	0.02	1.42	1.41	1.24	1.00	1.02	0.88	1.22	1.13	1.12	0.00	0.00	0.00	0.00	0.00	0.00	0.00
Mn	0.00	0.00	0.00	0.00	0.00	0.00	0.02	0.01	0.00	0.00	0.00	0.00	0.00	0.00	0.00	0.00	0.00	0.00	0.00	0.00	0.00	0.00
Mg	0.11	0.17	0.14	0.16	0.11	0.12	0.80	0.92	1.30	1.31	1.50	1.32	1.08	1.28	1.17	0.00	0.00	0.00	0.00	0.00	0.00	0.00
Ca	0.00	0.00	0.00	0.00	0.00	0.00	0.00	0.00	0.00	0.00	0.00	0.01	0.00	0.00	0.00	0.26	0.21	0.17	0.27	0.24	0.28	0.29
Na	0.05	0.03	0.14	0.10	0.05	0.04	0.01	0.01	0.03	0.03	0.02	0.00	0.01	0.02	0.02	0.74	0.80	0.78	0.72	0.74	0.70	0.68
K	0.96	0.96	0.80	0.86	0.90	0.95	1.01	1.02	0.79	0.86	0.85	0.88	0.90	0.96	0.99	0.01	0.01	0.00	0.00	0.01	0.02	0.01
X_{Mg}							0.36	0.40	0.51	0.57	0.59	0.60	0.47	0.53	0.51							
An %																26	21	18	27	24	28	30

4.3.2 *P–T* modelling

Modelled X_{Mg}, Grs, and Sps isopleths for cores, intermediate zones, and normal rims corresponding to the observed composition of garnet and biotite intersect in the Grt-Bt-Pl-Ms-Pg-Qtz-Rt-H_2O phase field (Fig. 7c). This is consistent with the assemblage present in the sample except for paragonite, which was not observed but is predicted to be present only in small amounts (< 2 modal %). The slightly lower Grs and higher X_{Mg} contents of the cores indicate that minor garnet zoning resulted from growth during an increase in pressure (Fig. 7c). Si content in muscovite was used to better constrain the pressure range due to the pressure-insensitive orientation of garnet isopleths in the phase field. Together with garnet compositions, the Si content of muscovite constrains conditions between 630 and 640 °C and between 11.7 and 13 kbar for the formation of the S_2 foliation (Fig. 7c), with cores forming between 11.7 and 12.2 kbar and intermediate zones and normal rims forming at up to ∼ 13 kbar. The higher Grs and lower X_{Mg} contents, and a similar Sps content in the rare thin rims on garnet, together with the growth of ilmenite rims on rutile, indicate retrogression to lower temperature, and probably lower pressure conditions (Fig. 7c). The lack of an older foliation in the sample or in the outcrop, and the zoning pattern of garnet leads us to interpret that the Vaddas Nappe was only affected by D_2 Caledonian metamorphism and subsequently retrogressed to lower *P–T* conditions.

4.4 Kåfjord Nappe (AR153)

4.4.1 Petrography and mineral chemistry

Sample AR153 (Figs. 2, 3; Table 1) is a medium- to fine-grained garnet-biotite-zoisite-schist sample taken from the lower Kåfjord Nappe. Biotite, muscovite, zoisite, and elongate quartz-feldspar aggregates define a strong mylonitic S_2 foliation (Fig. 4i). Muscovite generally occurs within the foliation grown together with biotite and as rare grains cross-cutting the S_2 foliation. Garnet is porphyroblastic and idiomorphic and sometimes has inclusion-rich cores and inclusion-poor rims. Cores include quartz, biotite, ilmenite, and chlorite (Fig. 4h). Chlorite is absent in the matrix. Rutile and titanite are both found as elongate grains parallel to the foliation, although rutile is significantly more abundant. Two generations of ilmenite occur as small inclusions in garnet and as thin rims on rutile grains (Fig. 4h, 4i). Garnet shows some compositional change from core to rim (Fig. 6c; Table 3). Alm content is variable across the garnet (between Alm_{53-62}). Grs content is around 19–21 mol % in the cores and increases towards the rims up to 22–26 mol %. In the profile (Fig. 6c), X_{Mg} does not vary much between cores and rims (0.15–0.18) although spot analyses show that X_{Mg} is often slightly lower in the cores than in the rims (Table 3). The Sps content is higher in the cores (3–5 mol %) than in the garnet rims (1–2 mol %). Plagioclase shows no zoning, and has a composition of An_{25} to An_{32}. The X_{Mg} in biotite is between 0.56 and 0.59. Si content of the white mica is between 3.16 and 3.2 (a.p.f.u.).

4.4.2 *P–T* modelling

Zoning in garnet and the difference between garnet inclusion assemblage and matrix assemblage reflect growth at evolving *P–T* conditions. The presence of chlorite and ilmenite as inclusions in garnet (Fig. 4h, i) indicates that the cores grew at different conditions relative to rims and the matrix, limiting core growth below 620 °C and 8.5 kbar. Garnet cores show a relatively higher Sps content and lower content of Grs than rims while X_{Mg} shows little variation between cores and rims. The sample was modelled under water saturated conditions and the resulting pseudosection is shown in Fig. 7d. The presence of chlorite and ilmenite as inclusions in garnet cores limits core growth conditions below 620 °C and 8.5 kbar. Modelled X_{Mg}, Grs, and Sps isopleths are consistent with measured garnet core composition within the Grt-Bt-Chl-Pl-Ilm-Qtz phase field, and constrains garnet core growth between 590 and 610 °C and between 5.5 and 6.8 kbar (Fig. 7d). The presence of rutile, zoisite, and muscovite in the matrix constrains formation of the S_2 foliation above 9 kbar in the Grt-Bt-Ms-Pl-Zo-Rt phase field, consistent with the matrix assemblage (Fig. 4i). Modelled X_{Mg}, Grs, and Sps isopleths representing measured garnet rim compositions constrain *P–T* conditions between 580 and 605 °C and between 9.2 and 10.1 kbar. The morphology of the isopleths is consistent with a lack of significant zoning in pyrope (and X_{Mg} content) in the garnets. A match with model compositions for the rim estimate is also observed with the measured plagioclase composition (Fig. 7d) and measured Si content in muscovite. The X_{Mg} value of biotite in the sample has a large range that is consistent with modelled values for both the garnet core and rim estimates, and which is likely the result of biotite growth and equilibration over evolving *P–T* conditions. There is no microstructural evidence to suggest that there is more than one generation of biotite. The shape of the garnet compositional profile (Fig. 6c) compared to the morphology of the isopleths on the pseudosection suggests initial garnet growth at low pressures followed by continuous garnet growth with increasing pressure (and slightly increasing temperature). Ilmenite rims on rutile grains are likely a result of later retrogression to lower pressures and temperatures.

4.5 Nordmannvik Nappe – migmatite (AR25b)

4.5.1 Petrography and mineral chemistry

Sample AR25b (Figs. 2, 3; Table 1) is a coarse-grained migmatitic paragneiss with leucosome segregations and dark restitic layers (Figs. 5e–f). The sample material used to determine bulk composition was trimmed of as much leucosome

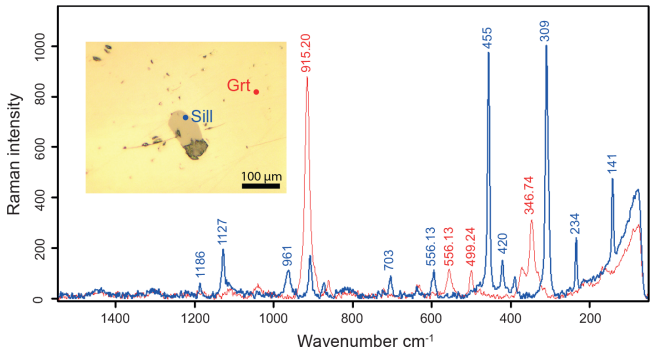

Figure 8. Raman spectra for a sillimanite inclusion from a garnet core in the Nordmannvik migmatite (sample AR25b).

as possible so that it contained ∼ 5–10 volume % leucocratic material. The sample has a macroscopic weak foliation defined by biotite and migmatitic banding. The leucosome consists of plagioclase, quartz, and K-feldspar (partly replaced by myrmekite). Kyanite and garnet porphyroblasts (2–3 mm in size) are common along leucosome boundaries and in the restite (Fig. 5f). Kyanite occurs as large (up to 6 mm) porphyroblasts oriented both randomly and parallel to the foliation and almost always in association with biotite, and often with quartz (Fig. 5f). Kyanite crystals sometimes contain inclusions of quartz and biotite, and are occasionally in contact with garnet. Smaller kyanite crystals are also found as inclusions in quartz in leucosomes. Garnet is usually idiomorphic, and contains inclusions of biotite, quartz, ilmenite, and sillimanite (the latter confirmed by Raman spectra; Figs. 8, 9a). In minor amounts, fine-grained sillimanite is intergrown with biotite or occurs along kyanite and garnet rims. Muscovite occurs as rare small grains overgrowing biotite and is often associated with fine-grained sillimanite. Garnets show a relatively flat compositional profile in the core and gradual changes near the rims, probably indicative of diffusion zoning. X_{Mg} in the cores is 0.23–0.26 and decreases to 0.20–0.23 in the rims. Alm in cores is between 65–69 mol % and 69–71 mol % in the rims. Grs in garnet cores is as low as 4.5 mol % and at the rims 6–7 mol %. Sps content of garnet cores is 3 mol % and 3.5–4 mol % in the rims (Fig. 9a).

4.5.2 *P–T* modelling

Metamorphic conditions for the migmatitic S_1 foliation in the Nordmannvik Nappe were estimated from sample AR25b (Fig. 10a). To set water content for migmatization, first an approximate pressure for equilibration was estimated from a water-saturated pseudosection using the XRF bulk composition. Isopleths for Grs, Sps, and X_{Mg} contents intersect at ∼ 10 kbar. The water content used in the pseudosection (Fig. 10a) was then determined from the position of the solidus on a T–X_{H_2O} pseudosection calculated at 10 kbar for the mineral assemblage associated with melting. The presence of kyanite and sillimanite, together with the variation in plagioclase and biotite composition, suggest that the minerals record evolving metamorphic conditions. The flat profile for garnet cores and changes at the rims suggest that the rims may have been modified by diffusion due to disequilibrium (Fig. 9a). The association of kyanite, biotite, and garnet with the leucosome in the S_1 foliation suggests that these minerals formed the stable assemblage during D_1 partial melting. Given the large volume of kyanite associated with the leucosome it can be explained by the following reaction: $Ms \pm Pl + Qtz = Kfs + Als + Liq$. This is consistent with the lack of muscovite in the rock and presence of K-feldspar. Based on the relationship between garnet rims and the leucosome, garnet rim compositions were taken as representative of the D_1 migmatization conditions.

Most measured garnet rim compositions and some intermediate zone compositions correspond with modelled isopleths in the phase field Grt-Bt-Pl-Kfs-Ky-Qtz-Melt on the pseudosection (Fig. 10a). X_{Mg}, Grs, and Sps contents from these analyses constrain D_1 partial melting between 760–790 °C and 9.4–11 kbar. Several measured garnet rims also correspond with modelled isopleths below the solidus within the muscovite-bearing assemblage, consistent with cooling, late muscovite growth, and late minor diffusional resetting of garnet rims. The minor fine-grained sillimanite with biotite and along kyanite and garnet rims is consistent with retrogression to lower pressures. The homogenous garnet core compositions were also plotted on the pseudosection (Fig. 10a) and modelled isopleths for Grs, Sps, and X_{Mg} contents correspond with measured contents in the sillimanite-bearing phase field (Grt-Bt-Pl-Kfs-Sill-Qtz-Melt) above the solidus between 790–815 °C and 8.9–9.9 kbar (Fig. 10a). These conditions correspond to the temperatures during D_1 melting, but at slightly lower pressures. The range in measured X_{Mg} content of biotite corresponds with isopleths that plot consistently with both estimates, whereas the measured anorthite content for matrix plagioclase corresponds with isopleths that plot toward the lower pressure conditions (sillimanite-bearing assemblage). It should be noted that the conditions estimated for garnet core formation may be affected by re-equilibration of the cores by later diffusion. Considering this, and given the presence of sillimanite inclusions in garnet, it is possible that garnet core conditions could have been up to ∼ 2–3 kbar lower pressure and ∼ 50 °C hotter than the predicted estimate based on their current composition.

4.6 Nordmannvik Nappe – mylonite (AR26)

4.6.1 Petrography and mineral chemistry

Sample AR26 (Figs. 2, 3; Table 1), which comes from just above the Nordmannvik–Kåfjord boundary, is a fine-grained garnet-kyanite micaschist that displays a pervasive mylonitic S_2 foliation defined by biotite, muscovite, and kyanite (Fig. 5b). It has a strong L_2 stretching lineation de-

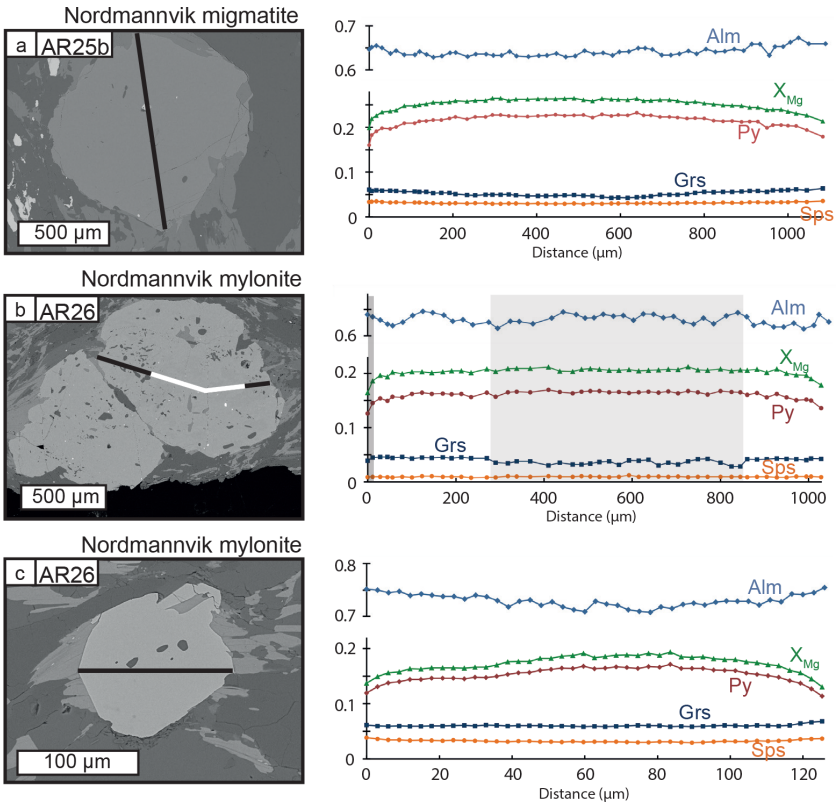

Figure 9. BSE images and garnet profiles for Nordmannvik Nappe samples AR25b and AR26. **(a)** Garnet in AR25b displays a profile with a steady increase in Alm, Grs, and Sps contents and decrease in Py and X_{Mg} towards garnet rims. **(b)** The garnet profile for the large garnet in sample AR26 displays a relatively flat profile with some compositional change towards the rims. An inclusion-free core, marked in grey on the profile and in white on the BSE image, shows slightly lower and more variable Grs content. **(c)** The garnet profile for small garnets in sample AR26 shows a steady increase in Alm, Grs, and Sps contents and steady decrease in Py and X_{Mg} contents towards the rims.

fined by quartz aggregates. Plagioclase locally forms 0.1–0.3 mm sized sigma clasts. Biotite occurs as two generations: less common large foliation-parallel grains, and as finer-grained elongate grains intergrown with muscovite. Muscovite occurs as mica fish parallel to the foliation, and as rare late grains that cross-cut the foliation (Fig. 5b). Garnet is found as large 1–2 mm idiomorphic porphyroblasts (Fig. 9b) that sometimes have inclusion-poor cores (with occasional sillimanite) and more inclusion-rich rims (quartz and biotite inclusions), and as small 0.1–0.4 mm idiomorphic grains that occur singularly (Fig. 9c) or as clusters oriented parallel to the S_2 foliation. The bimodal garnet grain size is also observed in hand specimens and is therefore not an artefact of sectioning.

The larger garnets (Fig. 9b) display a slight difference in composition relative to the smaller ones (Fig. 9c). Cores in the larger garnets have slightly lower Sps and Grs contents ($Sps_{1-1.5}$, Grs_{4-5}) than cores in the smaller garnets ($Sps_{2.5-3.5}$, Grs_{5-6}). Almandine content in the larger garnet cores (Alm_{71-76}) is higher than in the smaller garnet cores (Alm_{65-72}; Table 3). The larger garnets display a relatively flat profile with thin rims, while the smaller garnets exhibit more pronounce zoning (Fig. 9b, c). Inclusion-poor cores of the larger garnets appear microstructurally distinct from inclusion-rich rims; however, Grs is the only endmember that reflects this difference (Fig. 9b, grey box). The larger garnets have a thin 10–20 µm wide rim (Fig. 9b; dark-grey box) with lower X_{Mg} values and Grs contents than cores, whereas smaller garnets have a similar zoning profile, but lack the large flat cores. Based on the similarity in rim compositions, and the lack of a chemical zoning following the microstructure (inclusion free cores in large garnets), it appears that the slight compositional variations in both the large and small garnets probably resulted from diffusion during high-grade metamorphism. The smaller garnets are probably more completely re-equilibrated than the larger ones. The two generations of biotite have different compositions. Older biotite has an X_{Mg} between 0.56 and 0.58, closer to the composition of inclusions in garnet ($X_{Mg} \sim 0.6$). Younger biotite displays X_{Mg} values between 0.46 and 0.48. Plagioclase is un-zoned with a composition of 23–24 mol % (Table 4).

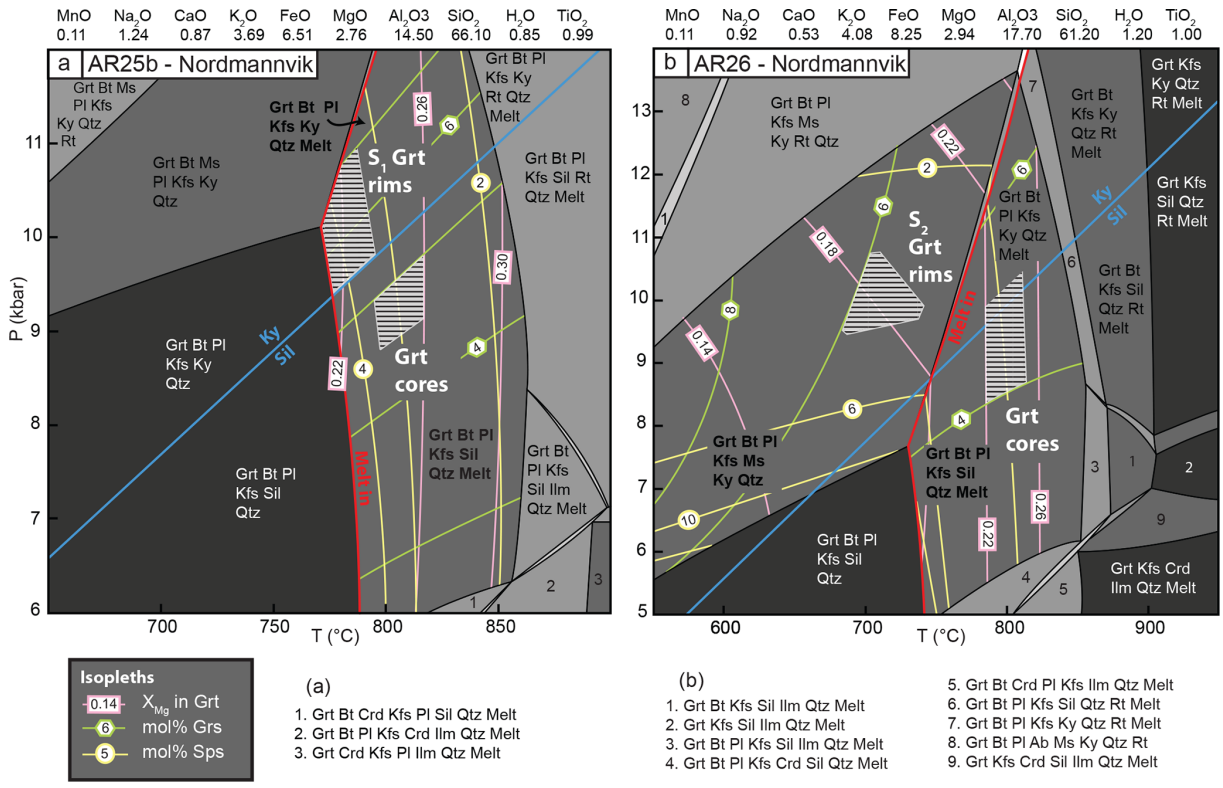

Figure 10. Pseudosections for the Nordmannvik Nappe. **(a)** Measured garnet core and rim compositions for migmatite (AR25b) agree with modelled compositions that plot above the solidus. Garnet cores give an apparent estimate in the sillimanite stability field. Garnet rims record S_1 foliation-related partial melting in the kyanite stability field. **(b)** Measured compositions of garnet cores and rims for S_2 mylonitic foliation (AR26) are shown. Garnet cores give an apparent estimate above the solidus in the sillimanite stability field (S_1 foliation – melting). Garnet rims and small garnets give an estimate below the solidus for the S_2 foliation.

4.6.2 *P–T* modelling

The variations in mineral compositions likely reflect changing *P–T* conditions with time. The profile shape and compositions of the larger and smaller garnets suggest that both probably started with the same homogenous composition and smaller garnets re-equilibrated more completely than large ones by diffusion during D_2 metamorphism and shearing (e.g. Caddick et al., 2010). Therefore, the cores of larger garnets may reflect the original *P–T* conditions. Biotite, kyanite, and muscovite are in contact with garnet rims and define a clear S_2 foliation associated with subsolidus shearing. X_{Mg}, Sps, and Grs compositions of the smaller re-equilibrated garnets and some larger garnet rims agree with modelled isopleths in the Grt-Bt-Pl-Kfs-Ms-Ky-Qtz phase field, and constrains the formation of the S_2 foliation between 680–730 °C and 9.5–10.9 kbar (Fig. 10b). Measured X_{Mg} values for the younger biotite generation and Si content in muscovite agree well with their respective modelled isopleths for this estimate. The Grs, Sps, and X_{Mg} contents of larger garnet cores (e.g. Fig. 9b, light-grey box) are consistent with modelled isopleths that plot within the Grt-Bt-Pl-Kfs-Ky-Qtz-Melt and Grt-Bt-Pl-Kfs-Sil-Qtz-Melt phase fields between 790–810 °C and 8–10.4 kbar (Fig. 10b). Although garnet core compositions have been affected by later diffusion and the rock has been strongly overprinted by the S_2 foliation, the estimated core conditions are consistent with those recorded by the migmatite sample (AR25b; Fig. 10a). This indicates that garnet cores record the same pre-D_2 history (D_1 melting and/or possibly earlier) reflected in the migmatites. The garnet core estimates agree with the presence of sillimanite inclusions in the cores, the measured X_{Mg} content of biotite inclusions in garnet, and anorthite content of plagioclase sigma clasts in the matrix, suggesting that garnet is not the only mineral that records this earlier *P–T* evolution.

5 Geochronology

In order to temporally constrain the metamorphic and deformation history of the RNC, zircon and titanite from several tectonic levels were selected for geochronology. The methods are described in supplement S1 and data are compiled in Supplement Tables 1–3.

5.1 D_1 melting in the Nordmannvik Nappe – U-Pb secondary ion mass spectrometry (SIMS) dating of zircon

Sample AR23a (Figs. 2, 3; Table 1) was taken from an S_1 lens in the Nordmannvik Nappe with clear leucosome segregations associated with kyanite-bearing restite. The sample was cut in an attempt to obtain different zircon populations for the restite and leucosome layers. Zircons from the restite are clear, euhedral, and prismatic crystals 100–350 µm long. All grains have low cathodoluminescence-emission (CL, dark grains) and show weak oscillatory zoning (Fig. 11a). Some grains have brighter rounded cores with discrete boundaries, indicative of a possible xenocrystic origin. Zircon from the leucosome is slightly larger than the grains from the restite. The grains are clear or yellow-orange in colour, and form euhedral prismatic crystals 150–350 µm long. Under CL they are equally dark and show similar weak oscillatory zoning to the zircon from the restite, but inherited cores are absent (Fig. 11d). For the restite, 37 spots were analysed in 26 grains. Five of the analyses are from the bright cores. These cores have Th/U ratios between 0.3–0.53. Two of the core analyses plot on concordia, two plot close by, and one is strongly discordant (Fig. 11b, grey ellipses). The discordant analysis is likely due to mixing of a CL-bright core and darker rim. Of the four analyses that plot on or near concordia, the oldest three give $^{207}Pb/^{206}Pb$ dates of 1836 ± 10, 1721 ± 10, and 1599 ± 14 Ma. The fourth core gives a younger $^{206}Pb/^{238}U$ date of 585 ± 8 Ma. The remaining 32 analyses are from regions in zircon grains that show low CL-emission and weak oscillatory zoning. They have Th/U ratios between 0.09 and 0.16, overlap on concordia, and give a combined concordia age of 441 ± 2 Ma (Fig. 11c). For the leucosome, 27 spots were analysed in 18 grains from both light and dark CL zones in the zircon crystals. They have Th/U ratios of 0.08 to 0.19, and form a cluster on concordia giving a concordia age of 439 ± 2 Ma (Fig. 11e). The concordia age for the leucosome is slightly younger than, although within error of, the restite concordia age. The oscillatory zoning patterns in the zircons from both the restite and leucosome populations and the shape of the zircons suggest they have crystallized from melt (e.g. Hoskin and Schaltegger, 2003).

5.2 Metamorphism in the Nordmannvik Nappe – U-Pb dating of titanite

Sample A01 is a coarse-grained felsic rock from a low-strain lens in the Nordmannvik Nappe on Arnøya (Figs. 2, 3, 11f, g; Table 1). The sample represents an interaction zone between melt and calc-silicate rocks and is composed of K-feldspar, quartz and plagioclase, and randomly oriented mafic schlieren that include mainly clinopyroxene, amphibole, plagioclase, biotite, quartz, and titanite with minor calcite, ilmenite, magetite, and iron sulphides. Only a weak macroscopic S_2 foliation is present (Fig. 11f). Titanite is abundant and coarse grained (up to 2 mm in size: Fig. 11g). It occurs as large euhedral grains mainly in the boundary zone between the schlieren and the felsic zones and is either associated with magnetite and quartz or as inclusions in the rims of amphibole grains. Sometimes it also occurs as thick rims on ilmenite. These microstructural relationships indicate it formed from interaction between melt and the calc-silicate rocks. Six clear-brown 300–600 µm sub- to euhedral titanite fragments were analysed using the thermal ionization mass spectrometry (TIMS) method. All analyses plot on concordia and four of them overlap (in bold; Fig. 11h) giving a combined concordia age of 432 ± 1 Ma. An older grain with a $^{206}Pb/^{238}U$ age of 440 ± 4 Ma and a younger grain with a $^{206}Pb/^{238}U$ age of 428 ± 1 Ma do not overlap with these analyses and these were not involved in the calculation of the concordia age. Together, these ages indicate a range between 440 ± 4 and 428 ± 1 Ma, with a peak at 432 ± 1 Ma.

5.3 Gabbro intrusion in the Vaddas Nappe – U-Pb SIMS dating of zircon

Sample SK18b was taken from a late-stage pegmatitic gabbro lens within the main medium-grained Kågen gabbro in the Vaddas Nappe (Figs. 2, 12a). It is coarse-grained and consists predominantly of up to 1 cm long amphibole crystals in a plagioclase matrix. Zircons from the sample are euhedral, short-prismatic, and between 100–300 µm long. CL zonation is variable. Twenty spots were analysed in 16 grains. Th/U values are between 0.3 and 0.7, consistent with zircon crystallization from a melt. All analyses are concordant giving a concordia age of 439 ± 1 Ma (Fig. 12c), interpreted as the intrusive age for late-stage gabbroic pegmatites within the Kågen gabbro.

5.4 S_2 shearing at the Vaddas–Kalak boundary – U-Pb titanite ages

Microstructural observations and P–T modelling show that titanite crystallization in sample UL248 is associated with the S_2 foliation during garnet rim growth (Figs. 4c, 6a). Titanite from the sample was therefore dated using TIMS. The majority of picked titanite grains have inclusions and the three cleanest fragments were chosen for analysis. They are pale-brown 240–300 µm long inclusion-free grains. All three analyses plot on Concordia with $^{238}U/^{206}Pb$ dates between 436 ± 4 and 431 ± 2 Ma (Fig. 12d). The mean $^{238}U/^{206}Pb$ age is calculated as 432 ± 6 Ma. We interpret this age to represent the age of D_2 shearing and metamorphism along the KNC–Vaddas boundary, and the likely emplacement age of the Vaddas Nappe over the KNC.

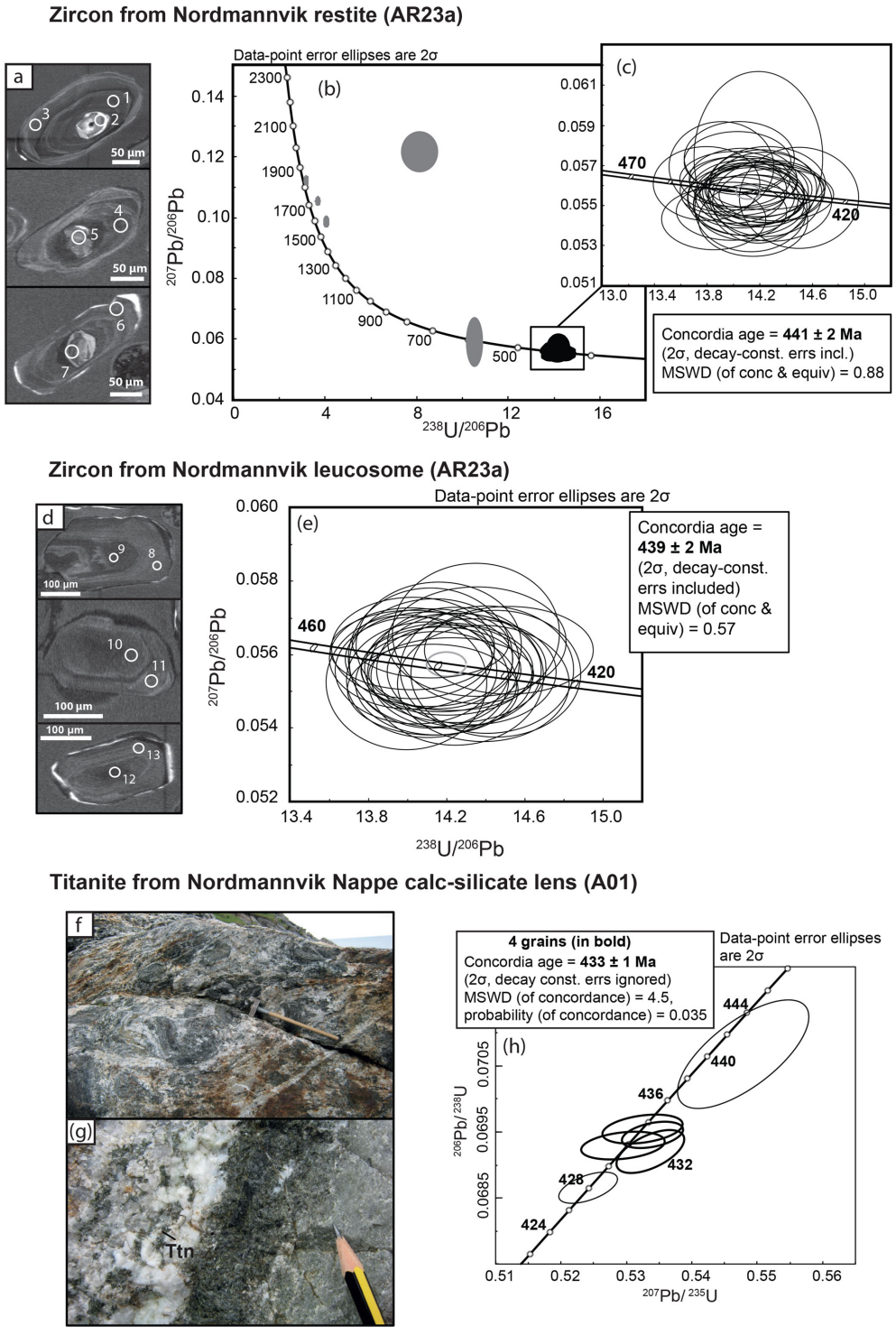

Figure 11. Age of partial melting and metamorphism in the Nordmannvik Nappe. **(a)** CL images of zircon grains with single spot analyses. $^{206}Pb/^{238}U$ dates for spot analyses are as follows: (1) 440 ± 5, (2) 585 ± 8, (3) 439 ± 5, (4) 441 ± 5, (5) 1421 ± 16, (6) 443 ± 5, and (7) 1547 ± 17 Ma. Note the presence of small, inherited cores. **(b)** Terra–Wasserburg diagram for SIMS zircon analyses from the restite of sample AR25b. Inherited core analyses are shown as grey ellipses. **(c)** Concordia diagram with age calculated for the young cluster of zircons in **(b)**. **(d)** CL images of zircon grains from the sample with single spot analyses. $^{206}Pb/^{238}U$ dates for spot analyses are as follows: (8) 441 ± 5, (9) 440 ± 5, (10) 441 ± 5, (11) 435 ± 5, (12) 438 ± 5, and (13) 434 ± 6 Ma. No inherited cores were observed in this sample. **(e)** Terra–Wasserburg diagram and concordia age for SIMS zircon analyses from the leucosome of sample AR25b. **(f)** Calc-silicate and leucosome mixing zone at sample site A01. **(g)** Close-up of calc-silicate and leucosome boundary showing titanite in a schlieren. **(h)** Concordia diagram for U-Pb TIMS analyses of titanites from a calc-silicate lens in the Nordmannvik Nappe (sample A01) with concordia age calculated for four overlapping analyses (in bold). The mean square of weighted deviates (MSWD) is also shown.

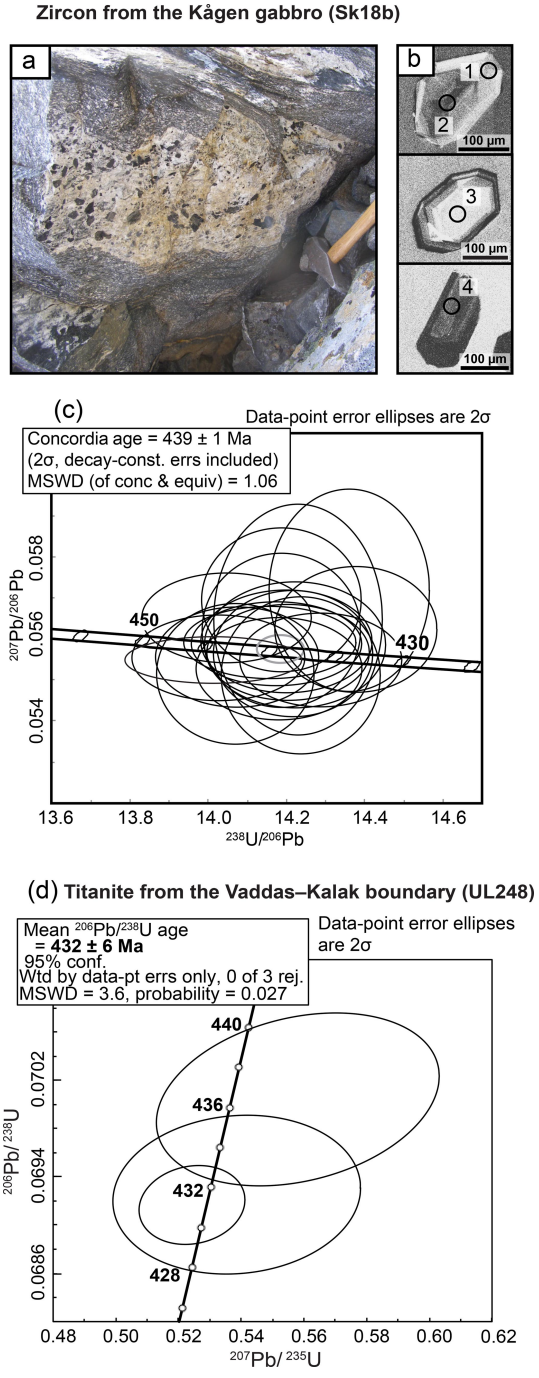

Figure 12. Ages related to intrusion and shearing in the Vaddas Nappe. **(a)** Photograph of the sampled gabbroic pegmatite (sample Sk18b); the hammer head is 15 cm long. **(b)** CL images of single zircon grains with spot analyses shown. The spot analyses have the following $^{206}Pb/^{238}U$ dates: (1) 438 ± 2.5, (2) 438.2 ± 2.7, (3) 439.1 ± 2.5, and (4) 444.4 ± 2.8 Ma. **(c)** Terra–Wasserburg diagram for SIMS zircon analysis from gabbroic pegmatite (sample SK18b) with Concordia age calculated showing the age of the Kågen gabbro intrusion into the Vaddas Nappe. **(d)** Concordia diagram for U-Pb TIMS analyses of titanites from the Vaddas–Kalak boundary (sample UL248) with mean $^{206}Pb/^{238}U$ age calculated.

6 Interpretation: metamorphic and magmatic evolution of the RNC

6.1 Potential Neoproterozoic metamorphic event in the KNC

Clear evidence for an early metamorphic event is preserved in sample UL248 from the KNC below the Vaddas–KNC boundary. Grt_1 (cores) formed between 705–735 °C and 9.9–10.8 kbar above the solidus (Fig. 7a) at higher temperature and lower pressure than Grt_2 (rims) (Figs. 7b, 13a). Sheared and dismembered leucosome suggests that melt solidified after an early melting event and was subsequently sheared in the solid state during the D_2 overprint. Age constraints for this early melting event are lacking. However, the metamorphic conditions for Grt_1 are similar to those recorded for partial melting in the KNC at Eide nearby ($\sim$ 730–775 °C and $\sim$ 6.3–9.8 kbar; Gasser et al., 2015; Fig. 13a, b). The Eide melting event is dated at 702 ± 5 Ma, indicating that it is of pre-Caledonian age (Gasser et al., 2015), and Caledonian migmatization has not been recorded in the KNC so far. We therefore suggest that Grt_1 in sample UL248 records the same pre-Caledonian partial melting recognized at Eide (Fig. 13b). Our results indicate that S_1 in the KNC is significantly older than S_1 in the RNC. The S_1-forming event in the KNC was termed D_1 by Gasser et al. (2015). It is not the same D_1 as we describe here in the RNC. In this paper we consider metamorphism in the KNC as pre-D_1 relative to the RNC.

6.2 Migmatization in the Nordmannvik Nappe – D_1

In the Nordmannvik Nappe early high-grade metamorphism is preserved as a S_1 migmatitic foliation in lower strain lenses. Phase equilibrium modelling of this foliation reveals that garnet cores in samples AR25b and AR26 reflect high-temperature mid- to low-pressure partial melting in the sillimanite and kyanite stability fields. The relationship between garnet cores and rims in migmatite sample AR25b and what the conditions estimated using the garnet core compositions might represent is difficult to interpret. The rim compositions are consistent with kyanite-present melting (ca. 760–790 °C and 9–11 kbar), whereas the cores indicate earlier lower pressure, higher temperature conditions (ca. 790–820 °C and 9–10 kbar; Figs. 10a, 13a). The lack of two distinct generations of garnet may suggest that their compositions record a single event. If this were the case, then the estimates constrained from core and rim compositions would record a single migmatization event, beginning at low pressures and continuing to higher pressures. The problem with such a scenario is that the melting reaction is almost completely temperature dependent, and therefore the bulk of melting would have occurred at the lower pressure sillimanite-present conditions with no or little melt produced at higher pressure. This is in contrast to the microstructures that suggest that substan-

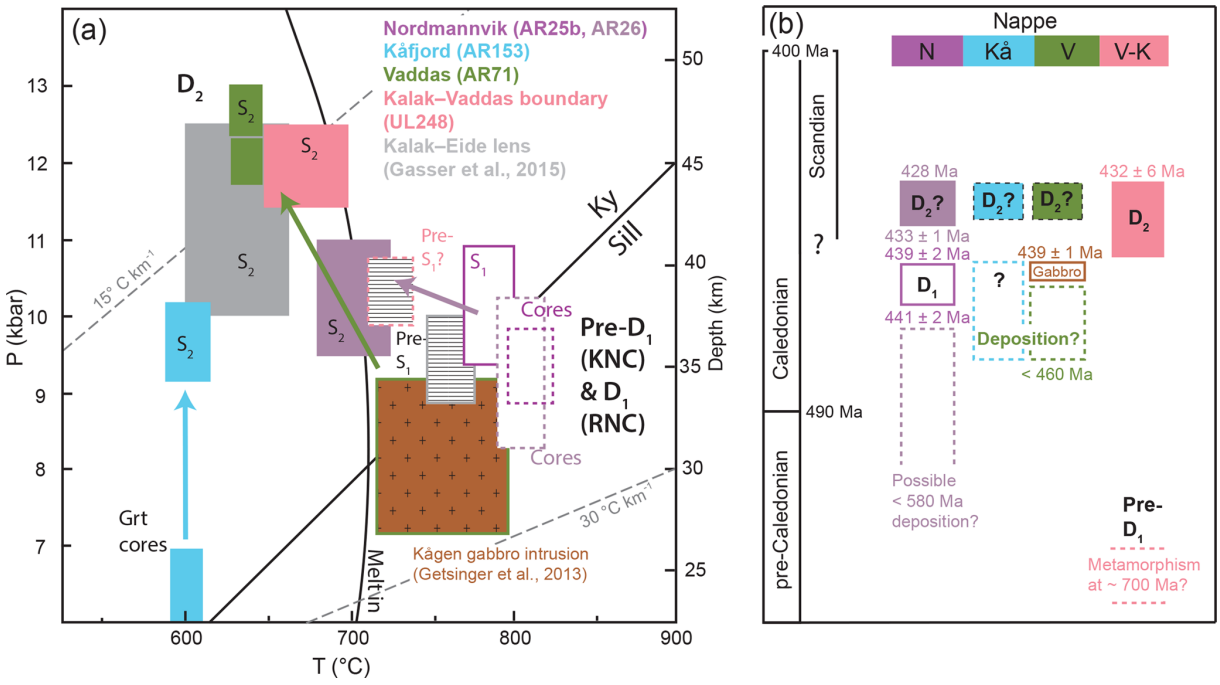

Figure 13. Summary of P–T conditions and timing for phase equilibrium modelling and geochronological results. **(a)** P–T diagram comparing conditions of metamorphism for pre-S_1 foliation garnet cores (striped boxes), D_1 migmatization (solid line box), apparent garnet core conditions in the Nordmannvik Nappe (dashed boxes), and S_2 foliation formation (shearing) (filled boxes) for all nappes. Estimated conditions for metamorphism in the KNC are shown in grey (Gasser et al., 2013). The intrusion conditions for the Kågen gabbro (brown box) are from Getsinger et al. (2013). Arrows show anticlockwise P–T paths for the Nordmannvik Nappe rocks and Vaddas or lower Kåfjord metasediments. **(b)** Timing of magmatism and metamorphism comparing ages across the nappes of the RNC and placing them within a pre-Caledonian and Caledonian context. Titanite ages are shown as filled boxes and zircon ages as solid-line boxes. Inferred and speculative ages are shown as dashed boxes.

tial partial melting produced mainly kyanite. This scenario is only possible if earlier melt formed under sillimanite-grade conditions removed from the system and melting continued under kyanite-grade conditions. However, due to high rates of diffusion in garnet that prevail at the temperatures under consideration during the D_1 partial melting and D_2 shearing (e.g. Caddick et al., 2010), we have to consider other possibilities for the metamorphism related to the sillimanite inclusions: (1) subsolidus prograde metamorphism related to D_1 migmatization, or (2) some unknown pre-D_1 (pre-Caledonian) event either above or below the solidus. Garnet cores in sample AR26 also record conditions above the solidus in the kyanite and sillimanite stability fields (ca. 790–810 °C and 8–10 kbar) prior to the D_2 shearing recorded by garnet rims (Figs. 10b, 13a). Polymetamorphism in the Nordmannvik Nappe has been previously related to Precambrian or Ordovician events (Elvevold et al., 1987; Lindstrøm and Andresen, 1992).

Leucosome associated with partial melting and formation of the kyanite-bearing S_1 foliation crystallized between 441 ± 2 and 439 ± 2 Ma (Figs. 11a–e, 13b). This indicates early Silurian melting at $\sim$ 30–37 km depth with a geothermal gradient of 22–25 °C km^{-1}. The presence of leucosome veins in the axial planes of Caledonian (F_2) folds in the Nordmannvik Nappe (Fig. 5d) indicates that the rocks were partially molten during folding. The rocks are also overprinted by the solid-state S_2 shear foliation (Fig. 5a, c). Considered together, these structures indicate that the Nordmannvik Nappe migmatites underwent initial deformation between 441 ± 2 and 439 ± 2 Ma while still partially molten, and continued shearing as the rocks solidified until the final D_2 overprinting took place in their solid state. This progression represents an anticlockwise P–T path (mainly with temperature decreasing) from D_1 to D_2 conditions (Fig. 13a). There is a large range in titanite dates (440 ± 4 to 428 ± 1 Ma) for the Nordmannvik migmatite sample A01, covering the age range of leucosome formation derived from zircon (between 441 ± 2 and 439 ± 2 Ma), but also extending to much younger dates. This range could be the result of either (1) diffusional Pb loss during cooling above the closure temperature of titanite (e.g. Tucker et al., 2004), or (2) protracted titanite growth (Kohn, 2017). The closure temperature of titanite is debated (e.g. Cherniak, 1993; Frost et al., 2001), although recent well constrained work in the Western Gneiss Region (WGR) suggests Pb diffusion in titanite is slow (Spencer et al., 2013; Kohn et al., 2015) and probably ineffective below 800 °C

(Kohn, 2017). The large grain size (> 300 µm) of the titanites in sample A01, and estimates for both D_1 and D_2 P–T conditions < 800 °C suggest it is unlikely that diffusional Pb loss caused the large age range, and from this we conclude that titanite probably grew over a protracted time period recording long-lived metamorphic processes.

The association of titanite and amphibole or titanite, magnetite, and quartz suggest that it formed by rehydration (1: $Cpx + Ilm + Qtz + H_2O = Amph + Ttn$) and/or oxidation (2: $Cpx + Ilm + O_2 = Ttn + Mag + Qtz$) reactions (e.g. Kohn, 2017) during crystallization of melt within calc-silicate layers. Both reactions are consistent with the observation of titanite rims on ilmenite grains. If both reactions were active, then prolonged titanite growth from ∼ 444 to 427 Ma in the Nordmannvik rocks probably resulted from switching between one reaction to the other during evolution of the system, controlled by H_2O and O_2 availability from injected melt and metamorphic fluids. Due to the chaotic migmatite structures the rocks do not demonstrate a clear S_2 shear foliation, but they record long-lived titanite growth probably driven by melt and/or fluid infiltration during prolonged early and peak Caledonian metamorphism. Both the zircon and titanite ages are consistent with the 439 ± 1 Ma metamorphic age (from zircon overgrowths) reported from the Nordmannvik Nappe at Heia (Augland et al., 2014).

6.3 Gabbro intrusion in the Vaddas Nappe

Coeval with the D_1 migmatization in the Nordmannvik Nappe, late-stage gabbroic pegmatites intruded the Vaddas Nappe on Kågen at 439 ± 1 Ma (Fig. 12c) at pressures between 7–9 kbar (Getsinger et al., 2013), corresponding to a depth of 26–34 km (Fig. 13). Getsinger et al. (2013) established the P–T range based on the presence of kyanite in syn-tectonic pegmatites related to gabbro intrusion, and on the composition of igneous biotite and metamorphic hornblende and plagioclase. The temperature range for intrusion is rather large (650–900 ± 50 °C), but the pressures are rather well constrained by the presence of zoisite at lower temperature shearing and kyanite in pegmatites (7–9 kbar). The data indicates a depth of intrusion of ∼ 26–34 km. The gabbroic composition clearly indicates a mantle source of the melt, and the tholeiitic composition, established from other mafic rocks and gabbros in the nappe (Lindahl et al., 2005), suggests melting in an extensional setting. The similar small gabbro bodies in the Kåfjord Nappe are probably also related to this event. The intrusion of the Kågen gabbro at 439 ± 1 Ma is slightly earlier than intrusion of the Heia gabbro in the Nordmannvik Nappe (435 ± 1 Ma; Augland et al., 2014).

6.4 Early garnet growth in the Kåfjord Nappe

Garnet cores in the sample from the lower Kåfjord Nappe (AR153) preserve lower amphibolite facies conditions (ca. 600 °C and 6–7 kbar; Figs. 7d, 13a). The P–T estimate is consistent with a slightly elevated geothermal gradient of 24–29 °C km^{-1}. Without direct age dating it is difficult to give the exact timing of this event. The lack of pre-D_2 structures in the lower Kåfjord metasediments and likely Late Ordovician depositional age constrains the time window for this metamorphism to either immediately prior to D_2 shearing or during early D_2 shearing (Fig. 13b). The P–T ratio indicates a similarity to the geothermal gradients estimated for D_1 migmatization and gabbro intrusion, suggesting that initial garnet growth in the Kåfjord Nappe may record the early Silurian heating event as in the Vaddas and Nordmannvik nappes, but at a shallower depth. Continuous garnet growth records the increase in pressure during D_2 shearing and eventually peak D_2 metamorphism.

6.5 Pervasive D_2 shearing

Pervasive amphibolite-facies D_2 shearing with top-to-SE kinematics is recorded throughout the entire RNC. KNC–Vaddas boundary rocks record D_2 shearing at ca. 630–690 °C and 11–12 kbar at similar conditions as D_2 shearing in the Vaddas Nappe (ca. 630–640 °C and 12–13 kbar; Figs. 7c, 13a), at depths around ∼ 43–46 km with the P–T ratio giving an estimated geothermal gradient of 14–15 °C km^{-1}. Garnets in the Kåfjord Nappe show an increase in pressure from 6 to 10 kbar at temperatures between 580 and 610 °C, reflecting a change in geothermal gradient from early high temperature and low pressure conditions to high pressure and low temperature conditions during D_2 shearing (Figs. 7d, 13a). In the Nordmannvik Nappe D_2 shearing is recorded in the mylonitic gneisses near the Kåfjord–Nordmannvik boundary at ca. 680–730 °C and 9–11 kbar (Figs. 10b, 13a). Although it is not possible to constrain uncertainties for individual P–T estimates, considering maximum possible errors, based on geological uncertainties, of ±50 °C and ±1 kbar (e.g. Palin et al., 2016), the P–T estimates for D_2 in the three nappes are similar, but with a trend towards the highest pressure at the base of the RNC, and the coldest temperature in the Kåfjord Nappe in the middle of the nappe stack (Fig. 13a). The age of D_2 shearing along the KNC–Vaddas boundary is constrained by syn-S_2 titanite to 432 ± 6 Ma (Figs. 12d, 13b), recording stacking of the Vaddas Nappe over the KNC. The age of D_2 metamorphism is consistent with ages for Caledonian metamorphism in the equivalent Magerøy Nappe (Andersen et al., 1982; Corfu et al., 2006, 2011; Kirkland et al., 2005, 2016), Narvik Nappe Complex (Augland et al., 2014) and upper KNC (Kirkland et al., 2007a; Gasser et al., 2015).

6.6 An anticlockwise P–T path for Caledonian metamorphism in the RNC

The Vaddas, Kåfjord, and Nordmannvik nappes all display an increase in pressure and/or decrease in temperature between pre-D_2 or early-D_2 high-temperature and low-pressure conditions and peak D_2 conditions of higher pressure and

lower temperature (Fig. 13a), recording a clear anticlockwise P–T path. Gabbro intrusion is syn-D_1 during high temperature and low pressure conditions at ca. 439 Ma. Although the Vaddas and Kåfjord metasediments do not exhibit partial melting (with the exception of locally around gabbro bodies), they also record this heating event. Anticlockwise metamorphism is recorded as the Nordmannvik Nappe migmatites solidified, between ca. 440–430 Ma, with an increase in pressure and decrease in temperature during Caledonian shearing (Figs. 13, 14). Although D_2 pressures in the Kåfjord Nappe are not as high as those in the Nordmannvik and Vaddas nappes, the shift of the Kåfjord Nappe from an environment with a higher geotherm towards one with a lower geotherm (Fig. 13a) is also consistent with an anticlockwise P–T path, recording crustal thickening and subduction of pre-heated rocks (but beginning in a shallower crustal position).

7 Discussion: the tectonic evolution of the RNC

7.1 Depositional ages

In order to understand the age–metamorphic–deformation relationships between the different nappes of the RNC and to reconstruct their tectonic evolution, the depositional ages of the metasedimentary rocks within the different nappes have to be known. As some of the metamorphic temperatures are so high that potential basement cover relationships cannot be reconstructed, the distinction between different nappes becomes difficult and can only be made on the basis of age dating or lithological associations. The Vaddas and Kåfjord samples are metasedimentary rocks that so far have not shown any evidence for a pre-Caledonian metamorphic or deformation history. The Magerøy Nappe, considered equivalent to the Vaddas Nappe, was sedimented in the earliest Silurian based on fossil evidence and an age of 438±4 Ma for volcaniclastic rocks, indicating deposition almost synchronously with emplacement of mafic–ultramafic and felsic magmas, and implying rapid burial of sediments (Andersen, 1981; Kirkland et al., 2005, 2016). Although no depositional ages for the Vaddas rocks associated with the dated gabbro have yet been obtained, the presence of Late Ordovician–early Silurian fossils at the base of the upper Vaddas metasediments south of the field area (e.g. Binns and Gayer, 1980) suggests that the upper Vaddas and possibly lower Kåfjord nappes in our study area are Late Ordovician or younger in age (Fig. 13b). The presence of sheared conglomerates at the base of the upper Vaddas Nappe (Figs. 3, 4d; Lindahl et al., 2005) suggests it was deposited on a continental basement; however, it is unclear what this basement was. The similarity of the metasediments in the lower Kåfjord Nappe, upper Vaddas Nappe and early Silurian volcaniclastic rocks of the Magerøy Nappe suggests that they might represent different stratigraphic and/or distal parts of the same Late Ordovician–early Silurian basin.

The upper Kåfjord rocks, displaying evidence for an S_1 foliation and an age of ca. 440 Ma for anatexis (Dangla et al., 1978) are different from the lower Kåfjord metasediments, and probably represent strongly sheared Nordmannvik-derived rocks. We therefore consider that the Kåfjord Nappe is probably comprised of sheared Nordmannvik-derived rocks in its upper part and sheared Vaddas-derived rocks in its lower part; however, the pervasive nature of S_2 foliation makes this difficult to define (Fig. 14b). The tectonostratigraphic position of the Nordmannvik paragneisses and their older zircon cores suggest they could also have been part of a more outboard basement to the Vaddas and Kåfjord metasediments (Fig. 15a–c). The protolith age of the Nordmannvik samples, however, is still unresolved. The presence of marble and calc-silicates suggests they were deposited as shallow water sediments, probably on a continental shelf. The oldest inherited zircon cores (ca. 1800–1600 Ma) may represent detrital ages from the original source rock, and are typical intrusive ages in northern Baltica (e.g. Larson and Berglund, 1992). The youngest inherited core age of 585 ± 8 Ma represents a maximum depositional age for these rocks (Figs. 11a, 13b). Farther to the south-west, the Narvik Nappe Complex, at the same tectonostratigraphic level, contains amphibolite-facies marbles with a chemostratigraphic depositional age of 610–590 Ma (Melezhik et al., 2014), indicating that the Nordmannvik rocks could indeed represent Late Neoproterozoic deposits.

7.2 Early Silurian (∼ 440 Ma) metamorphic and magmatic event

Prior to the development of top-to-SE S_2 foliation and shear zones, the KNC was the most inboard terrane relative to Baltica, with the lower Vaddas, upper Vaddas, Kåfjord, and Nordmannvik nappes increasingly more outboard (Figs. 14, 15). Based on pressure estimates for conditions prior to D_2 shearing, each nappe was also at different depths during this time, with the Kåfjord and Vaddas metasediments at mid- to lower-crustal levels, respectively, and the Nordmannvik rocks at high temperatures and pressures (lower-crustal level) during early Silurian heating (Fig. 14a). The garnet cores in the lower Kåfjord record a much higher structural level than the Vaddas rocks. Together, the relative positions and relationships between the different nappes in the Late Ordovician and Silurian suggests that the Vaddas and Kåfjord sediments were deposited in a continental basin (with KNC and/or possibly Nordmannvik basement) prior to early Silurian heating. The depth of gabbro intrusion requires that the Vaddas rocks were rapidly buried to ∼ 26–34 km depth by ca. 439 Ma, suggesting either a very deep basin or thickened continental crust facilitated by initial collision. Widespread intrusion of gabbro across all three nappes at different crustal levels indicates extensive early Silurian magma underplating.

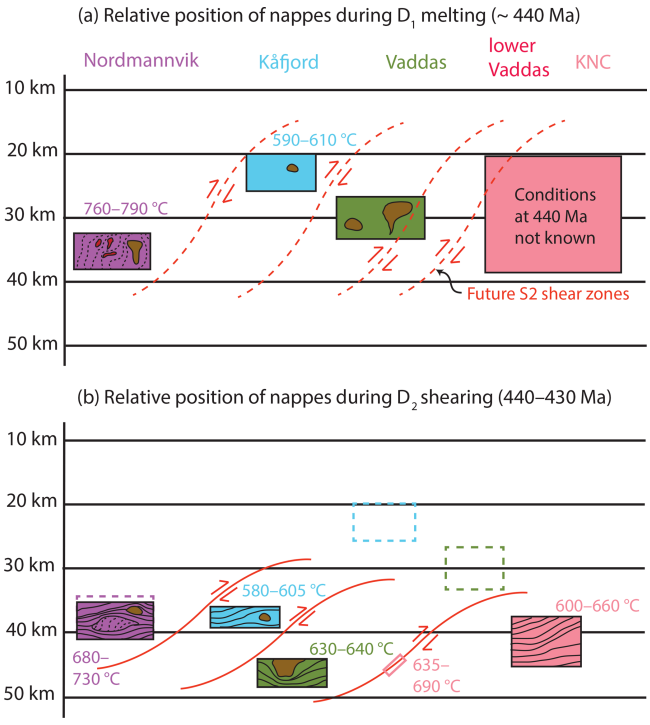

Figure 14. Relative positions and temperatures of the RNC nappes and KNC during **(a)** early Silurian heating (D_1 melting and gabbro intrusion) and **(b)** D_2 shearing, focussing on the sections through Arnøya and Uløya (lower Vaddas not present). D_1 conditions are shown in dashed, coloured boxes for comparison. In both **(a)** and **(b)** S_1 is shown as a dashed black line, and S_2 as a solid black line.

7.3 Similar early Silurian metamorphic and magmatic events in the Scandinavian Caledonides

Early Silurian migmatization in the Nordmannvik Nappe is similar to that observed in the Seve Nappe Complex (SNC), considered part of the outermost Baltica margin (continent–ocean transition zone). In the SNC, Ordovician high-pressure metamorphism (ca. 460 to 450 Ma) was followed by early Silurian (ca. 445–435 Ma) granulite facies metamorphism and magmatism (Gromet et al., 1996; Majka et al., 2012; Klonowska et al., 2013, 2017) at similar conditions to those recorded in the Nordmannvik Nappe. However, no evidence for Ordovician high-pressure metamorphism has been observed in the RNC (sillimanite inclusions in garnet suggest pre-Silurian high temperatures instead). The current lack of evidence for Ordovician high-pressure metamorphism in the RNC indicates that the RNC and SNC may have been in different tectonic positions relative to Baltica at that time.

Intrusive rocks of early Silurian age are widely recognized along the length of the Caledonides (e.g. Tucker et al., 1990; Gromet et al., 1996; Vaasjoki and Sipilä, 2001; Andréasson et al., 2003; Kirkland et al., 2005; Corfu et al., 2011; Majka et al., 2012; Klonowska et al., 2013, 2017). In northern Norway, they are found in the Narvik Nappe Complex (mafic Råå intrusion; 437 ± 0.5 Ma; Tucker et al., 1990), the Vaddas or Kalak Nappe (mafic Halti Igneous Complex; 434 ± 5 and 438 ± 5 Ma; Vaasjoki and Sipilä, 2001; Andréasson et al., 2003), and granitic and gabbroic rocks on Magerøy (intruded between 440–435 Ma; Kirkland et al., 2005; Corfu et al., 2011). The ages and tectonostratigraphic relationships established in this work support a correlation of the Narvik Nappe Complex with the Nordmannvik Nappe (e.g. Augland et al., 2014). The Magerøy Nappe has been most closely associated with the Vaddas Nappe (e.g. Andresen, 1988; Corfu et al., 2007). Both have similar lithologies and two-phase histories (D_1 and D_2 in the Magerøy Nappe; Andersen, 1981). Gabbro of the Honningsvåg igneous complex, which intrudes syn-D_1, has a similar age as the Kågen gabbro in the Vaddas Nappe (Corfu et al., 2006). The Skarsvåg Nappe overlies the Magerøy Nappe, is comprised of migmatitic mica-schist and quarzites, and is intruded by granites synchronously with or after D_1 at 436 ± 1 and 435 ± 2 Ma (Andersen, 1984; Corfu et al., 2006). The similarity in lithology, ages, structures, and tectonostratigraphy supports a correlation of the Magerøy Nappe with the Vaddas Nappe and overlying Skarsvåg Nappe with the Nordmannvik Nappe.

Early Silurian mafic magmatism is also recognized south at Sulitjelma and extensively within the Trondheim Nappe Complex (TNC; Fig. 1a; Pedersen et al., 1992; Nilsen et al., 2007; Slagstad and Kirkland, 2018). The age window of this mafic magmatism is between 438–434 Ma (Slagstad and Kirkland, 2018), fitting with the ages determined for the Kågen gabbro and migmatization in the Nordmannvik Nappe. Along the Caledonian orogen most occurrences are attributed to marginal basin settings, and typically considered as part of the Iapetus-derived rocks. In cases such as the TNC, oceanic rocks are recognized tectonostratigraphically below them (e.g. Andersen et al., 2012) in contrast to the RNC.

7.4 Large-scale tectonic models for the RNC

Several different tectonic scenarios have previously been proposed to explain the Ordovician high-pressure metamorphism and early Silurian mafic magmatism in the Scandinavian Caledonides (e.g. Pedersen et al., 1992; Northrup, 1997; Andréasson et al., 2003; Kirkland et al., 2005; Corfu et al., 2006; Slagstad and Kirkland, 2018). However, establishing tectonic models that fit rocks in northern Norway is challenging due to the lack of typical arc rocks, and oceanic rocks marking a suture. The only oceanic rocks present belong to the Lyngsfjellet Nappe, which overlies the RNC. The marked discontinuity in metamorphic grade between the Nordmannvik (amphibolite-granulite facies) and Lyngsfjellet (greenschist-low amphibolite facies) nappes suggests that the Lyngsfjellet Nappe was not thrust in sequence over the Nordmannvik Nappe, and that it did not reach the same depths as the RNC or KNC. The nature of the boundary between

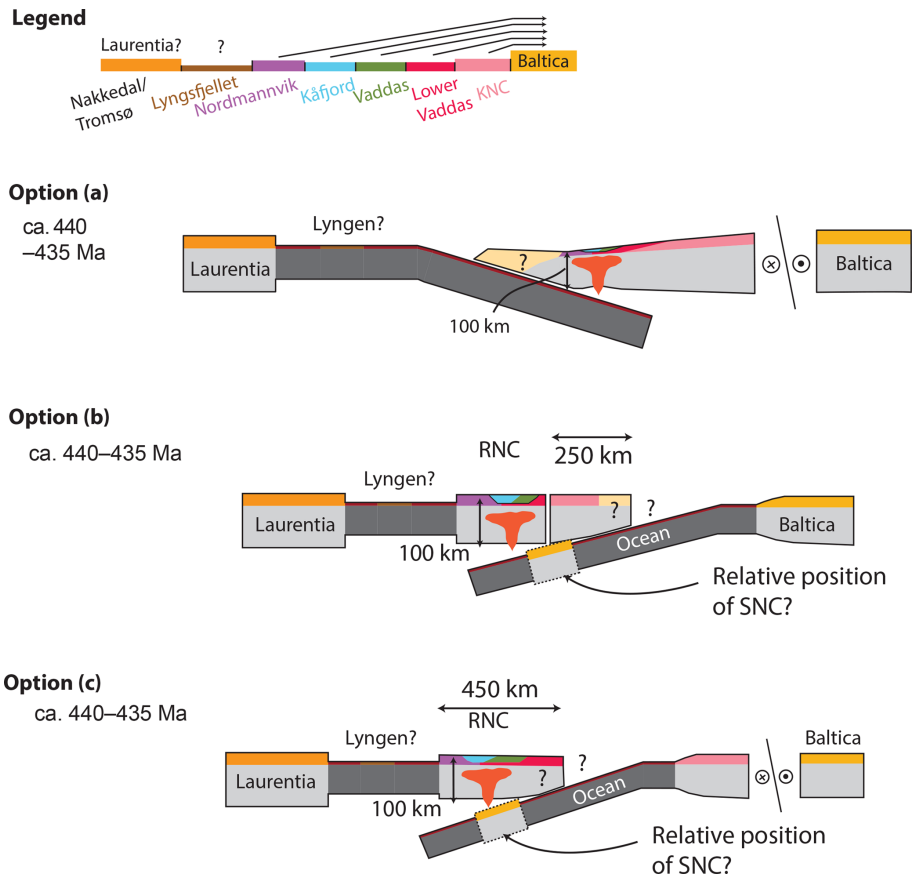

Figure 15. Diagram depicting some of the tectonic models discussed for the Caledonian nappes in the study area. The legend (top) shows the nappes in their relative palaeogeographic positions prior to D_2 nappe thrusting. Option **(a)** displays eastward-dipping subduction with the RNC as a back arc on an upper Baltica plate (e.g. Andréasson et al., 2003). Option **(b)** and **(c)** show westward-dipping subduction with the RNC in a back-arc position. Option **(b)** has the KNC on the upper plate, whereas option **(c)** has the KNC on the down-going plate.

the Nordmannvik Nappe and overlying Lyngsfjellet Nappe is still unclear, and it could also be a later detachment. Regardless, its position above the Nordmannvik Nappe means that it must have been somewhere outboard of the Nordmannvik Nappe rocks, with the overlying (possibly Laurentia derived) Nakkedal and Tromsø nappes representing more exotic elements during the early Silurian (Fig. 15; Corfu et al., 2003; Janák et al., 2012; Augland et al., 2014). The tectonostratigraphic position of the RNC suggests it formed a part of the outer Baltica margin (e.g. Fig. 15a).

Any tectonic model of the Caledonian evolution of the RNC in northern Norway needs to account for the tectonostratigraphy; Late Ordovician–early Silurian sedimentation and volcanism (Vaddas and Kåfjord); rapid burial and intrusion of tholeiitic gabbros (Vaddas) concurrent with migmatization in older, deeper rocks further outboard (Nordmannvik), followed by the onset of D_2 shearing; pressure increase and cooling (anticlockwise P–T path); and the development of a lower-crustal nappe stack. Anticlockwise P–T paths are typically observed where an initial heating event is followed by burial or cooling (Wakabayashi, 2004). Nappe stacking itself is not considered to be capable of providing the amount of heat required to explain the estimated temperatures for the initial heating event (e.g. Johnson and Strachan, 2006). Ridge subduction (e.g. Northrup, 1997; Corfu et al., 2006) has been mentioned as a possible explanation for the apparent coeval deposition of volcaniclastic sediments and tholeiitic mafic intrusions and the relatively short time window of mafic magmatism. However, the effect of ridge subduction on magmatism is usually very localized (e.g. Lomize and Luchitskaya, 2012) and does not explain the widespread nature of the early Silurian mafic magmatism several hundreds of kilometres along strike of the Caledonian orogeny from the Magerøy Nappe in the north to Trondheim in the south.

The widespread regional heating event is best explained by magmatic underplating of mantle melts. The gabbros with ~ 440 Ma intrusion ages (Kågen, Heia, Magerøy) are evidence for mantle melts at this time. Deposition of volcaniclastic sediments and tholeiitic mafic magmatism is often indicative of an extensional setting, such as a back-arc basin (e.g. Pedersen et al., 1992; Kirkland et al., 2005; Slagstad and Kirkland, 2018), and we consider this setting in several

different tectonic scenarios. Considering the RNC in a back-arc position on the Baltica margin would require eastward-dipping subduction (e.g. Fig. 15a; Andréasson et al., 2003). However, the KNC lacks the expected magmatism for this model, and there is no evidence for a switch in subduction polarity immediately prior to collision. For a back-arc environment we therefore have to consider that there is a missing suture below or within the RNC or KNC. Suture zones can be cryptic and difficult to identify in highly deformed rocks, with oceanic rocks typically not present along the entire length of a suture (Dewey, 1977). Similar nappes further south in the Caledonides display evidence for underlying oceanic rocks (e.g. Andersen et al., 2012).

Models that consider the RNC as formed in an extensional back-arc setting on the upper plate during westward subduction (e.g. Fig. 15b, c; cf. Slagstad and Kirkland, 2018) provide a good explanation for Ordovician–early Silurian deposition of volcanic rocks and sediments (Vaddas and Kåfjord) and intrusion of mafic rocks (e.g. Kågen gabbro; large-scale magma underplating), and provide an early Silurian heat source for an anticlockwise P–T path. The early collision and slab roll-back model of Slagstad and Kirkland (2018) supports short-lived early Silurian deposition, mafic magmatism and anticlockwise P–T path with rapid switching from extension and heating to compressional D_2 shearing (melt-filled D_2 axial planes in the Nordmannvik Nappe). However, palaeomagnetic data from the Honningsvåg igneous complex on Magerøy suggests it intruded the Magerøy Nappe rocks when they were $\sim$ 1350 km north of Baltica, supporting a possible early Silurian separation between Baltica and the RNC (e.g. Fig. 15b, c; Torsvik et al., 1992; Corfu et al., 2006).

Figure 15b and c offer two different scenarios based on the palaeogeographic position of the KNC. Both consider the Vaddas and Kåfjord having deposited in a back-arc basin on a continental basement. Option B places the KNC as an outboard microcontinent, while option C considers the KNC as part of the down-going plate. In this scenario the edge of the Baltica continent or some continent–ocean transition zone would have undergone subduction, consistent with Ordovician high pressure metamorphism in the SNC (Fig. 15a, b; e.g. Dallmeyer and Gee, 1986; Majka et al., 2014). Both scenarios require the presence of arc rocks either between the RNC and KNC or below the KNC. Traces of these arc rocks have not been found yet. It is possible that subduction was relatively short-lived, providing too little time for a proper arc to develop.

There are several problems that arise when considering the RNC rocks as having formed as part of a back-arc basin. The fairly high pressures of D_1 migmatization in the Nordmannvik Nappe (kyanite bearing; Fig. 13a) and deep-seated Kågen gabbro intrusion are not typical for an extensional environment, and intrusion of gabbro at 26 to 34 km depth into sediments in a back-arc basin requires a very deep basin, especially if it was short lived (e.g. Slagstad and Kirkland, 2018). The P–T path for D_2 shearing in the Vaddas and the near-isothermal increase in pressure from early heating to D_2 in the lower Kåfjord Nappe (Figs. 13a, 14) indicate subduction of pre-heated Vaddas rocks (deeper) and Kåfjord (shallower) as part of the lower plate. Some models discussed here fit better with our observations from northern Norway than others. Eastward-dipping subduction (e.g. Fig. 15a; Andréasson et al., 2003) seems unlikely or, at least, evidence for it is lacking so far. It is likely that the KNC (or at least its upper part) formed a microcontinent on the upper plate (e.g. Fig. 15b), placing the suture below it. The RNC as a microcontinent on the upper plate (e.g. Fig. 15c) is also a promising model, assuming that a yet unrecognized suture is present between the KNC and RNC. Both of these models (Fig. 15b, c) are possible in a scenario where early Silurian heating and gabbro intrusion resulted from extensive magma underplating in a back-arc setting with a rapid switch to shortening and collision over $\sim$ 10 million years. Discrepancies in the models could be due to uncertainties in observations (e.g. palaeomagnetic datasets or P–T estimates), or due to oblique collision, introducing strike-slip aspects to the story, and a possible overprinted pre-collisional accretion history.

The temperature and pressure evolution of the Vaddas and Kåfjord nappes from ca. 440 to 430 Ma can be used to discuss large-scale nappe stacking. Both indicate a clear pressure increase while temperatures remained similar (Fig. 14). An internal shear zone between the Kåfjord and Vaddas units was active to produce the thrust stacking of these two units (the pressure difference between them becomes more pronounced; Figs. 13a, 14). Both units combined show a pressure increase with respect to the Nordmannvik Nappe, which maintained its depth position (Figs. 13a, 14). This relative pressure development corresponds to thrusting of the Nordmannvik Nappe over the Vaddas and Kåfjord nappes or to initial subduction of these units underneath the Nordmannvik. The Vaddas Nappe was at the same depth as the KNC during the onset of this thrusting, together with the shear zone between them. This scenario suggests an initiation of a subduction zone towards the west with Kåfjord or Vaddas units at its leading edge or thrusting of the Nordmannvik Nappe over Kåfjord and Vaddas during continental collision.

8 Discussion: nappe stacking in continental collision zones

Even though the early Silurian tectonic history in northern Norway could have resulted from several different scenarios, the P–T evolution of the rocks indicates they formed a relatively hot and weak part of the middle to lower crust (especially the Nordmannvik Nappe) prior to Scandian nappe stacking (D_2; Fig. 13a). Additionally, D_2 deformation is pervasive and internal nappe strain can be as high as the strain along nappe boundaries. This is in contrast to typical Alpine-style nappes (e.g. Escher et al., 1993; Escher and Beau-

mont, 1997), where basement and cover relationships can be established on the basis of metamorphic grade or nappe dividers. It is also in contrast with anorthositic and granulitic Baltica crust in the WGR and Lofoten further south in Norway, which displays only very minor partial melting and little internal deformation, despite being subducted to depths > 100 km (Engvik et al., 2000; Hacker et al., 2010; Froitzheim et al., 2016). The anorthositic and granulitic rocks are not fertile or require large amounts of H_2O for partial melting. Conversely, the Nordmannvik rocks are fertile and show extensive partial melting. Caledonian deformation started under melt-present conditions (ca. 440 Ma) in a relatively high-temperature environment, then pressures increased and temperatures decreased from D_1 to D_2, constituting an anticlockwise P–T path. Subsequently, pervasive deformation continued into solid-state conditions (ca. 430 Ma). This suggests that initial high temperatures and associated partial melts played a key role in controlling the style of deformation at greater depth in continental collision zones: rock strength is significantly decreased even with melt fractions as low as $\sim 7\%$, and melt-bearing systems may facilitate strain localization (e.g. Rosenberg et al., 2005; Cavalcante et al., 2016). In northern Norway, the fertile Nordmannvik rocks are significantly different in composition compared to the dry, strong Baltica basement of the WGR and Lofoten. Partial melting in the fertile subducted Nordmannvik rocks led to strain localization and decoupling of nappe units from the crustal part of the lithosphere, and facilitated pervasive deformation (even in the internal parts of the nappes). Continental crust units are underthrusted and stacked as nappes (shown by increasing pressures in the Vaddas and KNC; Fig. 14b) instead of being subducted. This process destroys the integrity of the lithospheric slab and produces thin crustal nappe slivers. The initial high-temperature metamorphism and partial melting are critical to weakening processes in such a case. The response of the lithology to the metamorphic conditions exerts a key control on the strength of the rocks in a continental collision zone and can decide whether rocks become subducted or not and how they subsequently deform. In this way the structure, composition, and rheology of the lower crust during continental collision determines the geometry and kinematics during subduction of continental crust.

9 Conclusions

Our reported mineral assemblages, structures, and U-Pb dates from the RNC in northern Norway define a continuous sequence of events: (1) Late Ordovician–early Silurian sedimentation and mafic volcanism in the Vaddas and Kåfjord nappes; (2) early high-temperature partial melting in the Nordmannvik Nappe associated with a migmatitic fabric S_1 and mafic magmatism in the Vaddas, Kåfjord, and Nordmannvik nappes at 441 ± 2 to 439 ± 2 Ma, and 439 ± 1 Ma (D_1), respectively; followed by (3) pervasive amphibolite-facies shearing, formation of a subhorizontal S_2 foliation and L_2 lineation, and nappe stacking recorded at $\sim 432 \pm 6$ Ma (D_2). The transition from high-temperature medium-pressure D_1 metamorphism to higher-pressure lower-temperature D_2 metamorphism results in an anticlockwise P–T path. Deformation between these two events is continuous, and S_2 formation began while the rocks were still hot. The tectonic model that best accounts for our observations considers early Silurian heating resulting from extensive magma underplating in a back-arc system, followed rapidly (within 10 million years) by collision, crustal thickening, and nappe stacking. Early Silurian high temperature metamorphism in the RNC (particularly the Nordmannvik Nappe) led to weakening in the rocks, promoting extensive deformation, dismembering of the continental crust, and pervasive D_2 shearing during nappe stacking in early collision.

Data availability. Underlying data for this paper can be found in the supplement.

Supplement. The supplement related to this article is available online at: https://doi.org/10.5194/se-10-117-2019-supplement.

Author contributions. CF wrote most of the manuscript (with input from all co-authors), conducted $\sim 90\,\%$ of the field work, and gathered most of the data (XRF, EMP, SEM, SIMS, and TIMS) with assistance and input from the co-authors. CF, HS, DG, and PJ were involved in project design. Field data from Uløya, and XRF analysis, EMP analysis, and earlier phase equilibrium modelling for the sample from there (UL248) was conducted as part of the MSc project of KK. HS, DG, PJ, JK, and KK participated in the field work and discussions. JK and EKR gave advice on the phase equilibrium modelling, and EKR contributed previous knowledge of the rocks on Arnøya. FC assisted with sample preparation and TIMS analyses and contributed significantly to the discussion and the design of Fig. 15.

Competing interests. The authors declare that they have no conflict of interest.

Acknowledgements. We thank Luca Menegon for helpful discussions in the field. Christel Tinguely is thanked for help with the electron probe micro-analyzer (EMPA) at the University of Cape Town and Kai Neufeld for help with the SEM at UiT The Arctic University of Norway. SIMS data were collected at the Nordsim Laboratory, operated under an agreement between the research funding agencies of Denmark, Iceland, Norway, and Sweden; the Geological Survey of Finland; and the Swedish Museum of Natural History. Kerstin Lindén and Gavin Kenny assisted with the collection of SIMS data. This is NORDSIM publication no. 582. We thank UiT The Arctic University of Norway and the Norwegian Research School for Dynamics and Evolution of Earth

and Planets for supporting this work. The publication charges for this article have been funded by a grant from the publication fund of UiT The Arctic University of Norway. Very constructive reviews by Torgeir B. Andersen and Thorsten Nagel have improved the manuscript.

Edited by: Federico Rossetti
Reviewed by: Torgeir B. Andersen and Thorsten Nagel

References

Andersen, T. B.: The Structure of the Magerøy Nappe, Finnmark, North Norway, Norges. Geol. Unders., 363, 1–23, 1981.

Andersen, T. B.: The stratigraphy of the Magerøy Supergroup, Finnmark, North Norway, Norg. Geol. Unders. B, 395, 25–38, 1984.

Andersen, T. B., Austrheim, H., Sturt, B. A., Pedersen, S., and Kjærsrud, K.: Rb-Sr whole rock ages from Magerøy, North Norwegian Caledonides, Norsk Geol. Tids., 62, 79–85, 1982.

Andresen, A.: Caledonian terranes of northern Norway and their characteristics, Trabajos de Geologia, University of Oviedo, 17, 103–117, 1988.

Andresen, A. and Bergh, S.: Stratigraphy and tectonometamorphic evolution of the Ordovician-Silurian Balsfjord Group, Lyngen Nappe, north Norwegian Caledonides, The Caledonian Orogen – Scandinavia and related areas Part 1, 579–592, 1985.

Andresen, A. and Steltenpohl, M. G.: Evidence for ophiolite obduction, terrance accretion and polyorogenic evolution of the north Scandinavian Caledonides, Tectonophysics, 231, 59–70, https://doi.org/10.1016/0040-1951(94)90121-X, 1994.

Andréasson, P. G., Gee, D. G., Whitehouse, M. J., and Schöberg, H.: Subduction-flip during Iapetus Ocean closure and Baltica-Laurentia collision, Scandinavian Caledonides, Terra Nova, 15, 362–369, https://doi.org/10.1046/j.1365-3121.2003.00486.x, 2003.

Augland, L. E., Andresen, A., Gasser, D., and Steltenpohl, G.: Early Ordovician to Silurian evolution of exotic terranes in the Scandinavian Caledonides of the Ofoten-Troms area – terrane characterization and correlation based on new U-Pb zircon ages and Lu-Hf isotopic data, Geol. Soc. Spec. Publ., 390, 655–678, https://doi.org/10.1144/SP390.19, 2014.

Beaumont, C., Nguyen, M. H., Jamieson, R. A., and Ellis, S.: Crustal flow modes in large hot orogens, Geol. Soc. Spec. Publ., 268, 91–145, https://doi.org/10.1144/GSL.SP.2006.268.01.05, 2006.

Bertrand, M., Rapports des structures des Alpes de Glasis et du bassin bouiller du Nord, Soc. Géol. France Bull., 3, 318–330, 1884.

Binns, R. E. and Gayer, R. A.: Silurian or Upper Ordovician fossils of Goulasjavri, Norway, Nature, 284, 53–54, https://doi.org/10.1038/284053a0, 1980.

Caddick, M. J., Konopasek, J., and Thompson, A. B.: Preservation of garnet growth zoning and the duration of prograde metamorphism, J. Petrol., 51, 2327–2347, https://doi.org/10.1093/petrology/egq059 , 2010.

Cavalcante, G. C. G., Viegas, G., Archanjo, C. J., and da Silva, M. E.: The influence of partial melting and melt migration on the rheology of the continental crust, J. Geodyn., 101, 186–199, https://doi.org/10.1016/j.jog.2016.06.002, 2016.

Cherniak, D. J.: Lead diffusion in titanite and preliminary results on the effects of radiation damage on Pb transport, Chem. Geol., 125, 219–232, https://doi.org/10.1016/0009-2541(93)90253-F, 1993.

Chopin, C.: Ultrahigh-pressure metamorphism: tracing continental crust into the mantle, Earth Planet. Sc. Lett., 212, 1–14, https://doi.org/10.1016/S0012-821X(03)00261-9, 2003.

Coggon, R. and Holland, T. J. B.: Mixing properties of phengitic micas and revise garnet-phengite thermobarometers, J. Metamorph. Geol., 20, 683–696, https://doi.org/10.1046/j.1525-1314.2002.00395.x, 2002.

Connolly, J. A. D.: Computation of phase equilibria by linear programming: a tool for geodynamic modelling and its application to subduction zone decarbonation, Earth Planet. Sc. Lett., 236, 524–541, https://doi.org/10.1016/j.epsl.2005.04.033, 2005.

Corfu, F., Ravna, E. J. K., and Kullerud, K.: A late Ordovician U-Pb age for the Tromsø Nappe eclogites, Uppermost Allcohton of the Scandinavian Caledonides, Contrib. Mineral. Petrol., 145, 502–513, https://doi.org/10.1007/s00410-003-0466-x, 2003.

Corfu, F., Torsvik, T. H., Andersen, T. B., Ashwal, L. D., Ramsay, D. M., and Roberts, R. J.: Early Silurian mafic-ultramafic and granitic plutonism in comtemporaneous flysch, northern Norway: U-Pb ages and regional significance, J. Geol. Soc. London, 163, 291–301, https://doi.org/10.1144/0016-764905-014, 2006.

Corfu, F., Roberts, R. J., Torsvik, T. H., Ashwal, L. D., and Ramsay, D. M.: Peri-Gondwanan elements in the Caledonian nappes of Finnmark, northern Norway: implications for the paleogeographic framework of the Scandianvian Caledonides, Am. J. Sci., 307, 434–458, https://doi.org/10.2475/02.2007.05, 2007.

Corfu, F., Gerber, M., Andersen, T. B., Torsvik, T. H., and Ashwal, L. D.: Age and significance of Grenvillian and Silurian orogenic events in the Finnmarkian Caledonides, northern Norway, Can. J. Earth Sci., 48, 419–440, https://doi.org/10.1139/E10-043, 2011.

Corfu, F., Gasser, D., and Chew, D. M.: New perspectives on the Caledonides of Scandinavia and related areas: main features, conceptual advances and critical questions, Geol. Soc. Spec. Publ., 390, 9–43, https://doi.org/10.1144/SP390.25, 2014.

Dallmeyer, R. D. and Gee, D. G.: $^{40}Ar/^{39}Ar$ mineral dates from retrogressed eclogites within the Baltoscandian miogeocline: Implications for a polyphase Caledonian orogenic evolution, Geol. Soc. Am. Bull., 97, 26–34, 1986.

Dangla, P., Damange, J. C., Ploquin, A., Quarnardel, J. M., and Sonet, J.: Donn'es geochronologiques sur les Caledonides Scandinaves septentrionates (Troms, Norway du Nord), Cr. Acad. Sci. Paris, 286, 1.653–1.656, 1978.

Daly, J. S., Aitcheson, S. J., Cliff, R. A., Gayer, R. A. and Rice, A. H. N.: Geochronological evidence from discordant plutons for a late Proterozoic orogen in the Caledonides of Finnmark, northern Norway, J. Geol. Soc. London, 148, 29–40, https://doi.org/10.1144/gsjgs.148.1.0029, 1991.

Dewey, J. F.: Suture zone complexities: A review, Tectonophysics, 40, 53–67, https://doi.org/10.1016/0040-1951(77)90029-4, 1977.

Elvevold, S.: Petrologiske undersøkelse av Kaledonske bergater i Takvatnområdet, Troms, Masteroppgave, Universitetet i Tromsø, 1987.

Elvevold, S. and Andersen, T.: Fluid evolution during metamorphism at increasing pressure: carbonic- and nitrogen-bearing fluid inclusions in granulites from Øksfjord, north Norwe-

gian Caledonides, Contrib. Mineral. Petrol., 114, 236–246, https://doi.org/10.1007/BF00307758, 1993.

Elvevold, S., Reginiussen, H., Krogh, E. J., and Bjørklund, F.: Reworking of deep-seated gabbros and associated contact metamorphosed paragneisses in the southeastern part of the Seiland Igneous Province, northern Norway, J. Metamorph. Geol., 12, 539–556, https://doi.org/10.1111/j.1525-1314.1994.tb00041.x, 1994.

Engvik, A. K., Austrheim, H., and Andersen, T. B.: Structural, mineralogical and petrophysical effects on deep crustal rocks of fluid-limited polymetamorphism, Western Gneiss Region, Norway, J. Geol. Soc. London, 157, 121–134, https://doi.org/10.1144/jgs.157.1.121, 2000.

Escher, A. and Beaumont, C.: Formation, burial and exhumation of basement nappes at crustal scale: a geometric model based on the Western Swiss-Italian Alps, J. Struct. Geol., 19, 955–974, https://doi.org/10.1016/S0191-8141(97)00022-9, 1997.

Escher, A., Masson, H., and Steck, A.: Nappe geometry in the Western Swiss Alps, J. Struct. Geol., 15, 501–509, https://doi.org/10.1016/0191-8141(93)90144-Y, 1993.

Froitzheim, N., Miladinova, I., Janák, M., Kullerud, K., Ravna, E. K., Majka, J., Fonseca, R. O. C., and Münker, C.: Devonian subduction and syncollisional exhumation of continental crust in Lofoten, Norway, Geology, 44, 223–226, https://doi.org/10.1130/G37545.1, 2016.

Frost, B. R., Chamberlain, K. R., and Schumacher, J. C.: Sphene (titanite): phase relations and role as a geochronometer, Chem. Geol., 172, 131–148, https://doi.org/10.1016/S0009-2541(00)00240-0, 2001.

Fuhrman, M. L. and Lindsley, H.: Ternary-feldspar modeling and thermometry, Am. Mineral., 73, 201–215, 1988.

Gasser, D., Jerabek, P., Faber, C. Stünitz, H., Menegon, L., Corfu, F., Erambert, M., and Whitehouse, M. J.: Behaviour of geochronometers and timing of the metamorphic reactions during deformation at lower crustal conditions: phase equilibrium modeling and U-Pb dating of zircon, monazite, rutile and titanite from the Kalak Nappe Complex, northern Norway, J. Metamorph. Geol., 33, 513–534, https://doi.org/10.1111/jmg.12131, 2013.

Gayer, R. A. and Roberts, J. D.: Stratigrahic review of the Finnmark Caledonides, with possible tectonic implications, Proc. Geol. Soc., 84, 405–428, https://doi.org/10.1016/S0016-7878(73)80023-9, 1973.

Gee, D. G., Andréasson, P. G., Li, Y., and Krill, A.: Baltoscandian margin, Sveconorwegian crust, lost by subduction during Caledonian collisional orogeny, GFF, 139, 36–51, https://doi.org/10.1080/11035897.2016.1200667, 2017.

Gerya, T. V. and Meilick, F. I.: Geodynamic regimes of subduction under an active margin: effects of rheological weakening by fluids and melts, J. Metamorph. Geol., 29, 7–31, https://doi.org/10.1111/j.1525-1314.2010.00904.x, 2010.

Getsinger, A. J., Hirth, G., Stünitz, H., and Georgen, E. T.: Influence of water on rheology and strain localization in the lower continental crust, Geochem. Geophy. Geosy., 14, 2247–2264, https://doi.org/10.1002/ggge.20148, 2013.

Gromet, L. P., Sjöström, H., Bergman, S., Claesson, S., Essex, R. M., Andréasson, P. G., and Albrecht, L.: Contrasting ages of metamorphism in the Seve nappes: U-Pb results from the central and northern Swedish Caledonides, Geol. Foren. Stock. For., 118, 37–38, https://doi.org/10.1080/11035899609546308, 1996.

Hacker, B. R., Andersen, T. B., Johnston, S., Kylander-Clark, A. R. C., Peterman, E. M., Walsh, E. O., and Young, D.: High-temperature deformation during continental-margin subduction and exhumation: The ultra-high pressure Western Gneiss Region of Norway, Tectonophysics, 480, 149–171, https://doi.org/10.1016/j.tecto.2009.08.012, 2010.

Holland, T. and Powell, R.: Calculation of phase relations involving haplogranitic melts using an internally consistent thermodynamic dataset, J. Petrol., 42, 673–683, https://doi.org/10.1093/petrology/42.4.673, 2001.

Holland, T. J. B. and Powell, R.: An internally consistent thermodynamic data set for phases of petrological interest, J. Metamorph. Geol., 16, 309–343, https://doi.org/10.1111/j.1525-1314.1998.00140.x, 1998.

Hollister, L. S. and Crawford, M. L.: Melt-enhanced deformation: A major tectonic process, Geology, 14, 558–561, 1986.

Hoskin, P. W. O. and Schaltegger, U.: The composition of zircon and igneous and metamorphic petrogenesis, Rev. Mineral. Geochem., 53, 27–62, https://doi.org/10.2113/0530027, 2003.

Janák, M., Ravna, E. J. K., and Kullerud, K.: Constraining peak P-T conditions in UHP eclogites: calculated phase equilibria in kyanite- and phengite-bearing eclogite of the Tromsø Nappe, Norway, J. Met. Petr., 30, 377–396, https://doi.org/10.1111/j.1525-1314.2011.00971.x, 2012.

Jeřábek, P., Lexa, O., Schulmann, K., and Plašienka, D.: Inverse ductile thinning via lower crustal flow and fold-induced doming in the West Carpathian Eo-Alpine collisional wedge, Tectonics, 31, TC5002, https://doi.org/10.1029/2012TC003097, 2012.

Johnson, M. R. W. and Strachan, R. A.: A discussion of possible heat sources during nappe stacking: the origin of Barrovian metamorphism within the Caledonian thrust sheets of NW Scotland, J. Geol. Soc. London, 163, 579–582, https://doi.org/10.1144/0016-764920-168, 2006.

Kirkland, C. L., Daly, J. S., and Whitehouse, M. J.: Early Silurian magmatism and the Scandian evolution of the Kalak Nappe Complex, Arctic Norway, J. Geol. Soc. London, 162, 985–1003, https://doi.org/10.1144/0016-764904-124, 2005.

Kirkland, C. L., Daly, J. S., and Whitehouse, M. J.: Granitic magmatism of Grenvillian and late Neoproterozoic age in Finnmark, Arctic Norway – constraining pre-Scandian deformation in the Kalak Nappe Complex, Precambr. Res., 145, 24–52, https://doi.org/10.1016/j.precamres.2005.11.012, 2006.

Kirkland, C. L., Daly, J. S., Eide, E. A., and Whitehouse, M. J.: Tectonic evolution of the arctic Norwegian Caledonides from a texturally- and structurally- constrained multi-isotopic (Ar-Ar. Rb-Sr, Sm-Nd, U-Pb) study, Am. J. Sci., 307, 459–526, https://doi.org/10.2475/02.2007.06, 2007a.

Kirkland, C. L., Daly, J. S., and Whitehouse, M. J.: Provenance and terrane evolution of the Kalak Nappe Complex, Norwegian Caledonides: implications for Neoproterozoic paleogeography and tectonics, J. Geol., 115, 21–41, https://doi.org/10.1086/509247, 2007b.

Kirkland, C. L., Daly, J. S., and Whitehouse, M. J.: Basement-cover relationships of the Kalak Nappe Complex, Arctic Norwegian Caledonides and constraints on Neoproterozoic terrane assembly in the North Atlantic region, Precambr. Res., 160, 245–276, https://doi.org/10.1016/j.precamres.2007.07.006, 2008.

Kirkland, C. L., MacGabhann, B. A., Kirkland, B. L., and Daly, J. S.: Cryptic disc structures resembling Edi-

acaran discoidal fossils from the lower Silurian Hellefjord Schist, Arctic Norway, PloS ONE, 11, e0164071, https://doi.org/10.1371/journal.pone.0164071, 2016.

Klonowska, I., Majka, J., Janák, M., Gee, D. G., and Ladenberger, A.: Pressure-temperature evolution of a kyanite-garnet pelitic gneiss from Åreskutan: evidence of ultra-high pressure metamorphism of the Seve Nappe Complex, west-central Jämtland, Swedish Caledonides, Geol. Soc. Spec. Publ., 390, 321–336, https://doi.org/10.1144/SP390.7, 2013.

Klonowska, J., Janák, M., Majka, J., Petrík, I., Froitzheim, N., Gee, D. G., and Sasinková, V.: Microdiamond on Åreskutan confirms regioal UHP metamorphism in the Seve Nappe Complex of the Scandinavian Caledonides, J. Metamorph. Geol., 35, 541–564, https://doi.org/10.1111/jmg.12244, 2017.

Kohn, M. J.: Titanite petrochronology, Rev. Mineral. Geochem., 83, 419–441, https://doi.org/10.2138/rmg.2017.83.13, 2017.

Kohn, M. J., Corrie, S. L., and Markley, C.: The fall and rise of metamorphic zircon, Am. Mineral., 100, 897–908, https://doi.org/10.2138/am-2015-5064, 2015.

Kvassnes, A. J. S., Strand, A. H., Moen-Eikeland, H., and Pedersen, R. B.: The Lyngen Gabbro: the lower crust of an Ordovician Incipient arc, Contrib. Mineral. Petrol., 148, 358–379, https://doi.org/10.1007/s00410-004-0609-8, 2004.

Labrousse, L., Hetenyi, G., Raimbourg, H., Jolivet, L., and Andersen, T. B.: Initiation of crustal-scale thrusts triggered by metamorphic reactions at depth: Insights from a comparison between the Himalayas and Scandinavian Caledonides, Tectonics, 29, TC5002, https://doi.org/10.1029/2009TC002602, 2010.

Larson, S. A. and Berglund, J.: A chronological subdivision of the Transscandinavian Igneous Belt – three magmatic episodes?, Geol. Foren. Stock. For., 114, 459–461, https://doi.org/10.1080/11035899209453912, 1992.

Lindahl, I., Stevens, B. P. J., and Zwaan, K. B.: The geology of the Vaddas area, Troms: a key to our understanding of the Upper Allochton in the Caledonides of northern Norway, Norg. Geol. Unders. B, 445, 5–43, 2005.

Lindstrøm, M. and Andresen, A.: Early Caledonian high-grade metamorphism within exotic terranes of the Troms Caledonides?, Norsk Geol. Tids., 72, 375–379, 1992.

Lomize, M. G. and Luchitskaya, M. V.: Subduction of spreading ridges as a factor in the evolution of continental margins, Geotectonics, 46, 47–68, https://doi.org/10.1134/S0016852112010049, 2012.

Majka, J., Be'eri-Shelvin, Y., Gee, D. G., Ladenberger, A., Claesson, S., Konečy, P., and Klonowska, I.: Multiple monazite growth in the Åreskutan migmatite: evidence for a polymetamorphic Late Ordovician to Late Silurian evolution in the Seve Nappe Complex of west-central Jämtland, Sweden, J. Geosci., 57, 3–23, https://doi.org/10.3190/jgeosci.112, 2012.

Majka, J., Rosén, Å., Janák, M., Froitzheim, N., Klonowska, I., Manecki, M., Sasinková, V., and Yoshida, K.: Microdiamond discovered in the Seve Nappe (Scandinavian Caledonides) and its exhumation by the "vacuum-cleaner" mechanism, Geology, 42, 1107–1110, https://doi.org/10.1130/G36108.1, 2014.

Melezhik, V. A., Kuznetsov, A. B., Pokrovsky, B. G., Solli, A., Gorokhov, I. M., Fallick, A. E., Lindahl, I., Konstantinova, G. V., and Melnikov, N. N.: Chemostratigraphic insight into deposition of the Melkedalen Marble, Narvik Nappe Complex, North-Central Norwegian Caledonides, Norw. J. Geol., 94, 35–52, 2014.

Nilsen, O., Corfu, F., and Roberts, D.: Silurian gabbro-diorite-trondhjemite plutons in the Trondheim Nappe Complex, Caledonides, Norway: petrology and U-Pb geochronology, Norw. J. Geol., 87, 329–342, 2007.

Northrup, C. J.: Timing structural assembly, metamorphism, and cooling of the Caledonian Nappes in the Ofoten-Efjord area, North Norway: tectonic insights from U-Pb and $^{40}Ar/^{39}Ar$ geochronology, J. Geol., 105, 565–582, https://doi.org/10.1086/515958, 1997.

Palin, R. M., Weller, O. M., Waters, D. J., and Dyck, B.: Quantifying geological uncertainty in metamorphic phase equilibria modelling; a Monte Carlo assessment and implications for tectonic interpretations, Geosci. Front., 7, 591–607, 2016.

Pedersen, R. B., Bruton, D. L., and Furnes, H.: Ordovician faunas, island arcs and ophiolites in the Scandinavian Caledonides, Terra Nova, 4, 217–222, https://doi.org/10.1111/j.1365-3121.1992.tb00475.x, 1992.

Pfiffner, O. A.: Basement-involved thin-skinned and thick-skinned tectonics in the Alps, Geol. Mag., 153, 1085–1109, https://doi.org/10.1017/S0016756815001090, 2016.

Ramsay, D. M., Sturt, B. A., Zwaan, K. B., and Roberts, D.: Caledonides of Northern Norway, in: The Caledonian Orogen – Scandinavia and Related areas, edited by: Gee, D. G. and Sturt, B. A., New York, Wiley, 163–184, 1985.

Rice, A. H. N.: Stretching lineations and structural evolution of the Kalak Nappe Complex (Middle Allochton) in the Repparfjord-Fægfjord area, Finnmark, northern Norway, Norsk Geol. Tids., 78, 277–289, 1998.

Rice, A. H. N.: Restoration of the external Scandinavian Caledonides, Finnmark, North Norway, Geol. Soc. Spec. Publ., 390, 271–299, https://doi.org/10.1017/S0016756816000340, 2014.

Roberts, D.: Geologisk kart over Norge, berggrunnskart, Hammerfest 1:250 000, Norges Geologiske Undersøkelse, 1973.

Roberts, D. and Gee, D. G.: An introduction to the structure of the Scandinavian Caledonides, in: The Caledonian Orogen – Scandinavia and Related areas, edited by: Gee, D. G. and Sturt, B. A., Wiley, Chichester, 55–68, 1985.

Roberts, D. and Sturt, B. A.: Caledonian deformation in Norway, J. Geol. Soc. London, 137, 241–250, https://doi.org/10.1144/gsjgs.137.3.0241, 1980.

Robins, B.: The mode of emplacement of the Honningsvåg Intrusive Suite, Magerøya, northern Norway, Geol. Mag., 135, 231–244, 1998.

Rosenberg, C. L. and Handy, M. R.: Experimental deformation of partially melted granite revisited: implications for the continental crust, J. Metamorph. Geol., 23, 19–28, https://doi.org/10.1111/j.1525-1314.2005.00555.x, 2005.

Schardt, H.: Sur l'origine des Prealpes romandes, Eclogae Geol., Helvetiae, 4, 129–142, 1893.

Schreyer, W., Ohnmacht, W., and Mannchen, J.: Carbonate-orthopyroxenites (sagvandites) from Troms, northern Norway, Lithos, 5, 345–364, https://doi.org/10.1016/0024-4937(72)90089-8, 1972.

Schulte-Pelkum, V., Monslave, G., Sheehan, A., Pandey, M.R., Sapkota, S., Bilham, R., and Wu, F.: Imaging the Indian subcontinent beneath the Himalaya, Nature, 435, 1222–1225, https://doi.org/10.1038/nature03678, 2005.

Slagstad, T. and Kirkland, C. L.: Timing of collision initiation and location of the Scandian orogenic suture in the Scandinavian Caledonides, Terra Nova, 0, 1–10, https://doi.org/10.1111/ter.12324, 2018.

Spencer, K. J., Hacker, B. R., Kylander-Clark, A. R. C., Andersen, T. B., Cottle, J. M., Stearns, M. A., Poletti, J. E., and Seward, G. G. E.: Campaign-style titanite U–Pb dating by laser-ablation ICP: Implications for crustal flow, phase transformations and titanite closure, Chem. Geol., 341, 84–101, https://doi.org/10.1016/j.chemgeo.2012.11.012, 2013.

Spengler, D., Brueckner, H. K., Roermund, H. L. M., Drury, M. R., and Mason, P. R. D.: Long-lived, cold burial of Baltica to 200 km depth, Earth Planet. Sc. Lett., 281, 27–35, https://doi.org/10.1016/j.epsl.2009.02.001, 2009.

Stephens, M. B. and Gee, D. G.: Terranes and polyphase accretionary history in the Scandinavian Caledonides, in: Terranes in the Circum-Atlantic Paleozoic Orogens, edited by: Dallmeyer, R. D., Geol. Soc. Am. Spec., 230, 17–30, 1989.

Streule, M. J., Strachan, R. A., Searle, M. P., and Law, R. D.: Comparing Tibet-Himalayan and Caledonian crustal architecture, evolution and mountain building processes, Geol. Soc. Spec. Publ., 335, 207–232, https://doi.org/10.1144/SP335.10, 2010.

Tajčmanová, L., Connolly, J. A. D., and Cesare, B.: A thermodynamic model for titanium and ferric iron solution in biotite, J. Metamorph. Geol., 27, 153–165, https://doi.org/10.1111/j.1525-1314.2009.00812.x, 2009.

Torsvik, T. H., Olesen, O., Trench, A., Andersen, T. B., Walderhaug, H. J., and Smethurst, M. A.: Geophysical investigation of the Honningsvåg igneous complex, Scandinavian Caledonides, J. Geol. Soc. London, 149, 373–381, https://doi.org/10.1144/gsjgs.149.3.0373, 1992.

Tucker, R. D., Boyd, R. D., and Barnes, S. J.: A U-Pb zircon age for the Råna intrusion, N, Norway: new evidence of basic magmatism in the Scandinavian Caledonides in Early Silurian time, Norsk Geol. Tids., 70, 229–239, 1990.

Tucker, R. D., Robinson, P., Solli, A., Gee, D. G., Thorsnes, T., Krogh, T. E., Nordgulen, O., and Bickford, M. E.: Thrusting and extension in the Scandian hinterland, Norway: New U-Pb ages and tectonostratigraphic evidence, Am. J. Sci., 304, 477–532, https://doi.org/10.2475/ajs.304.6.477, 2004.

Vaasjoki, M. and Sipilä, P.: U-Pb isotope determinations on baddeleyite and zircon from the Halti-Ridnitsohkka intrusion in Finnish Lapland: a further constraint on the Caledonide evolution, Geol. S. Finl., 33, 247–253, 2001.

Wakabayashi, J.: Tectonic mechanisms associated with P-T paths of regional metamorphism: alternatives to singe-cycle thrusting and heating, Tectonophysics, 392, 193–218, https://doi.org/10.1016/j.tecto.2004.04.012, 2004.

Whitney, D. L. and Evans, B. W.: Abbreviations for names of rock-forming minerals, Am. Mineral., 95, 185–187, https://doi.org/10.2138/am.2010.3371, 2010.

Zhao, Z., Mo, X., Dilek, Y., Niu, Y., DePaolo, D. J., Robinson, P., Zhu, D., Sun, C., Dong, G., Zhou, S., Luo, Z., and Hou, Z.: Geochemical and Sr-Nd-Pb-O isotopic compositions of the post-collisional ultrapotassic magmatism in SW Tibet: Petrogenesis and implications for India intra-continental subduction beneath southern Tibet, Lithos, 113, 190–212, https://doi.org/10.1016/j.lithos.2009.02.004, 2009.

Zwaan, K. B. and Roberts, D.: Tectonostratigraphic succession and development of Finnmarkian Nappe sequence, North Norway, Norg. Geol. Unders. B, 343, 53–71, 1978.

Zwaan, K. B.: Nordreisa, berggrunnsgeologisk kart – M 1 : 250 000, Norges geologiske unerdsøkelse, 1988.